INFLUENCE OF IMMERSED CONDUCTIVE OBJECTS ON THE BURNING BEHAVIOR OF OIL SOAKED SAND

by

Shivaprasad Arava

A Thesis

Submitted to the Faculty

of the

WORCESTER POLYTECHNIC INSTITUTE

in partial fulfillment of the requirements for the

Degree of Master of Science

in

Mechanical Engineering

July 2016

APPROVED:

_____

Professor Ali S. Rangwala, Advisor

_____

Professor V Raghavan, IIT – M(India), Committee member

_____

Dr. Hayri Sezer, WPI, Committee member

_____

Dr. Kemal Sarp Arsava, WPI, Committee Member

_____

Professor Cosme Furlong, Graduate Committee Representative

Abstract

The objective of this study is to characterize the flammability of oil-soaked sand towards the development of technology to clean up petroleum product spills using *in situ* combustion. The burning rate of a sand-oil mixture is enhanced using immersed conductive objects (copper rods) which enable rapid heat-up of the flame exposed to the upper surface of the rod and transmits heat back into the sand. Consequent conduction of heat to the porous media through the lower portion of the immersed rod significantly increases vaporization and therefore the burning rate. Bench scale experiments ($10cm$) were performed with increasing spill content (18% and 24%) exposed to external heat fluxes (15, 20, 25 and 30$\frac{kW}{m^2}$) and different rod configurations (single rod, multiple rods and cases with various heights and diameters). Flammability parameters such as ignition time, mass loss rate, and temperature profiles were investigated. Experiments show that the ignition time decreases and the burn efficiency rate increases with the addition of immersed objects. A numerical model is used to further explain the controlling parameters for enhancement in burning rate and optimization of the technique.

Acknowledgement

I would first like to thank my thesis advisor, Prof. Ali S Rangwala for his guidance, support and great patience at all times. I would like to express my gratitude to Prof Raghavan (IIT-M, India) for the useful comments, remarks, and engagement through the learning process of this master thesis. I am also grateful to Dr. Hayri Sezer for helping me in understanding the heat transfer and numerical code for the experiments. Furthermore, I would like to thank Dr. Kemal Sarp Arsava for introducing me to the topic as well for the support on the way.

I take this opportunity to thank my friend, Apoorv Walawalkar for helping me in conducting experiments and for the sleepless nights we had while working together.

I also thank the combustion lab manager, Trevor Borth in guiding and helping me with the test setup and also allowing me to conduct experiments during late nights. I am grateful to have Lydia Shi, Mahesh Kottalagi, Aravind Krishnan, Samim Safaei, Panyawat Tukaew, Raymond Ranellone, Shijin Puthiyaparambath Kozhumal, David Petrow, and Sreenivasan Ranganathan as my lab mates, who helped me in all time in sharing space, time and also helping me with the thesis.

Finally, I would also like to thank my parents, brothers, grandparents and friends who are thousands of miles apart and continuously encouraging me with wishes.

Table of Contents

Abstract i
Acknowledgement ii
List of Tables v
List of Figures vi
Nomenclature viii
Chapter 1 1
1.1 Introduction 1
1.2 Motivation 2
1.3 Literature Review 2
1.3.1 History of crude oil spills 3
1.3.2 Clean-up methods for crude oil spill 6
1.3.3 *In situ* burning of crude oil spills on sand: 12
Chapter 2 17
2.1 Methodology 17
2.2 Experimental Setup 17
2.2.2 Experimental matrix 21
2.2.3 Baseline cases 22
2.2.4 Cases with single immersed rod 23
2.2.5 Cases with multiple immersed rods 24
2.2.6 Cases with higher rod height and lower rod diameter 25
Chapter 3 28
3.1 Results 28
3.1.1 Ignition time 28
3.1.2 Mass loss 30
3.1.3 Temperature profiles 36
3.1.4 Emissions from fuel mixtures 37
3.2 Discussions 40
Chapter 4 48
4.1 Mathematical model 48
4.1.1 Problem description 50

4.1.2 Finite Volume method for two-dimensional unsteady conduction 50
4.2 Model Assumptions 54
4.3 Model results 54
Chapter 5 58
Conclusions & Future work 58
References 59
APPENDIX A 63

List of Tables

Table 1: List of major crude oil spills [17] 5
Table 2: ANS Crude oil properties [34] 19
Table 3: Ignition time for fuel mixture (18% of emulsion & 82% sand) 29
Table 4: Ignition time for fuel mixture (24% of emulsion & 76% sand) 29
Table 5: 200g fuel composition 30
Table 6: 190g fuel composition 31
Table 7: Mass loss of fuel (18% of emulsion with 82% sand) 31
Table 8: Mass loss of fuel (24% of emulsion with 76% sand) 32
Table 9: Mass loss (%) for case (a) 35
Table 10: Mass loss (%) for case (b) 35
Table 11: Ignition Temperature for 18% Emulsion and 82% sand (case (a)) 37
Table 12: Ignition Temperature for 24% Emulsion and 76% sand (case (b)) 37
Table 13: Thermal properties of materials used in experiments [34, 37-43] 49

List of Figures

Figure 1: In-situ burning at Refugio County, Texas [15] 4
Figure 2: In-situ burning at Chiltpin Creek, Texas [15] 5
Figure 3: Manual cleanup method using shovel and other machinery [18] 7
Figure 4: Crude oil spill clean-up using boom 8
Figure 5: Clean up using skimmers [19] 9
Figure 6: Oil spill clean-up using chemical dispersants [20] 10
Figure 7: Biodegradation method of oil spill clean-up [21] 11
Figure 8: In-situ burning of crude oil spill [22] 12
Figure 9: Schematic diagram of small scale apparatus for smoldering process [31] 15
Figure 10: (a) before mixing with coal tar (b) after mixing with coal tar and (c) after smoldering [31] 16
Figure 11: Experimental setup 18
Figure 12: Before Emulsification 20
Figure 13: Cone heater Calibration curve 21
Figure 14: Experimental Matrix 22
Figure 15: Baseline test setup 23
Figure 16: Single immersed rod setup 24
Figure 17: Multiple Immersed rods - test setup 25
Figure 18: Increased height of rod test setup 26
Figure 19: Test setup for multiple immersed rods (Ø-0.45cm) 27
Figure 20: Cross-sectional view of burnt fuel at 25 kW/m^2 heat flux 33
Figure 21: Top view of burnt fuel at 25 kW/m^2 heat flux 34
Figure 22: CO_2 emission from 18% emulsion and 82% sand mixture burnt at 15 $kWm2$ heat flux 39
Figure 23: CO emission from 18% emulsion and 82% sand mixture burnt at 15 kW/m^2 heat flux 40
Figure 24: Comparison of ignition time 41
Figure 25: Comparison of mass loss 42

Figure 26: Fuel mixture burning at different time interval for single immersed copper rod test setup (heat flux- 15kW/m^2, case (a)) 42
Figure 27: Fuel mixture burning at different time interval for multiple immersed copper rods test setup (heat flux- 15kW/m^2, case (a)) 43
Figure 28: Temperature distribution in fuel at 100s 44
Figure 29: Temperature distribution inside the fuel at 200s 45
Figure 30: Temperature distribution inside the fuel at 600s 46
Figure 31: Temperature distribution inside the fuel at 800s 47
Figure 32: Schematic representation of the porous fuel geometry and the extracted computational cell for control volume approach (baseline) 51
Figure 33: Schematic representation of the porous fuel geometry and the extracted computational cell for control volume approach (immersed rod) 51
Figure 34: Schematic representation of temperature distribution inside fuel bed for baseline and immersed rods case for 18% emulsion and 82% sand at 15kW/m^2 55
Figure 35: Schematic representation of temperature distribution inside fuel bed for baseline and immersed rods case for 18% emulsion and 82% sand at 30kW/m^2 55
Figure 36: Schematic representation of temperature distribution inside fuel bed for baseline and immersed rods case for 24% emulsion and 76% sand at 15kW/m^2 56
Figure 37: Schematic representation of temperature distribution inside fuel bed for baseline and immersed rods case for 24% emulsion and 76% sand at 30kW/m^2 56
Figure 38: Schematic representation of temperature plots at different locations inside the fuel mixture for 18% emulsion with 82% sand 57

Nomenclature

H_f	flame height [m]
CV	control volume
T	temperature [K]
$\dot{q}''$	heat flux [W.m^{-2}]
h	convection heat transfer coefficient [W.m^{-2}.K^{-1}]
k	thermal conductivity [W.m^{-1}.K^{-1}]
$\dot{m}$	mass loss rate [g.s^{-1}]
c_p	specific heat at constant pressure [J.kg^{-1}.K^{-1}]
ρ	density [kg.m^{-3}]
A	area [m^2]
L_H	heater length [m]
L_c	collector length [m]
N_x, N_y and N_z	number of grids in x, y, and z directions respectively
°C	degree centigrade
°F	degree Fahrenheit
°K	Degree Kelvin
m	mass (g)
g	gravity constant [m.s^{-2}]
Subscripts	
o	oil
$cond$	conduction
$conv$	convection
rad	radiation
os	object surface
f	flame
F	Fuel
∞	ambient
sat	saturation

Chapter 1

1.1 Introduction

Clean up of hazardous spills during extraction, transport, and handling of petroleum products is a significant environmental concern. Depending on the geographical location of the spill different forms of clean up procedures are usually deployed by industry to remove the contaminant efficiently from the ecosystem and cause minimum damage to the habitat. Such cleanup methods include [1]:

a. Mechanical: Booms, Skimmers, Sorbents

b. Chemical: dispersants

c. Physical: *In situ* Burning

d. Biological: Bioremediation

The focus of the current study is to identify the controlling parameters related to *in situ* burning (ISB)[2], specifically in circumstances related to petroleum products spilled over a porous medium such as sand, pebbles, etc. A new technique of using an immersed metallic copper cylinder to enhance the heat transport into the sand bed is tested for the first time and shows promising results both in the enhancement of burning rate as well as the reduction in emissions. Alaska North Slope (ANS) crude oil is chosen for the study. Further, to create a worst-case scenario (for combustion) the ANS crude oil is mixed with water (60% by mass) to form a relatively dilute mixture incapable of ignition in a baseline case comprising of the oil-water mixture in an open pan. A series of experiments are performed in a small-scale experimental apparatus (~10 cm diameter) to characterize the burning behavior of oil-water mixtures soaked in the sand at different concentrations with the presence of metallic cylinders. The implications of ISB and incineration technologies for efficient cleanup of oil-soaked sand in remote areas is discussed.

1.2 Motivation

A similar study has been done with liquid media by Rangwala et al. [3]. This study developed a safe, low emission, burner to quickly burn an oil-water emulsion recovered from a skimming system. 'Flame Refluxer'^{TM} (a conductive metal rod used to transfer radiative and convective heat generated by combustion back to fuel) used to increase burning rate. Experiments conducted in 3 different phases based on the diameter of the burner, small scale (0.1m), intermediate-scale (0.5 m) and large-scale tests (1 m). The height of the flame refluxer, number of flame refluxer were optimized. These experiments were performed by varying the composition of the emulsion.

Flame Refluxer showed a significant increase in the burning rate for all the three different phases; the small scale showed an enhancement of 330% with single flame refluxer and 1250% with multiple flame refluxer. In the intermediate scale, the efficiency of burning increased by 280% with all different emulsions. Finally, in the large scale of 1m diameter burner, burning efficiency increased by 600% compared to the baseline case[1].

With these results, it provided a motivation to conduct a study on the influence of conductive materials in burning porous media with emulsions.

1.3 Literature Review

This section consist of three parts; a) history of oil spills, b) oil spill clean-up methods and c) In-situ burn method to clean offshore oil spills.

[1] Baseline experiments are with no flame refluxer

1.3.1 History of crude oil spills

Exxon Valdez oil spill: In 1989, at Prince William Sound, Alaska. A ship carrying 53,094,510 gallons of crude oil transported by the Trans-Alaskan pipeline, spilled crude oil because of wellhead blowout. Around 20% that is, 10.8 million gallons of crude oil spilled on water and spreading over an area of 1100 square miles [4]. Clean up of spilled oil performed by various methods. 20% of the oil evaporated and underwent photolysis[2]. 50% biodegradation and in-situ, 14% recovered or disposed and remaining were subtidal sediments. Total cleaning took around a year and a half with cost estimating $2.5 billion [5].

Santa Barbara California (1969): During an offshore drilling by union company near Santa Barbara coastline, California [6]. Crude oil could not be extracted from a 3500-feet-deep well. A pressure difference in the pump was not enough to drill, and this pressure difference ruptured the pipeline resulting in a spill of 3 million gallons[4].

Santa Barbara California (2015): On May 17, 2015, near Refugio state beach in Santa Barbara County, California [7]. A pipeline owned by Plains All American, transporting oil from Santa Barbara to Texas. Hundred and forty-two thousand eight hundred gallons of crude oil spilled [8] and spread over an area of 7 square miles. Leakage in pipeline found to be not having automatic shutdown valves and rupture due to corrosion. The 28-year-old pipeline not inspected for the past three years before the spill took place. Due to corrosion, walls of pipe were thinning and resulted in rupturing. This spill was much smaller compared with the previously mentioned spill at Santa Barbara but had a significant impact on ecology and environment.

Deepwater Horizon oil spill [9]: On 20th April 2010, a spill took place in the Gulf of Mexico. The oil rig owned by a company named BP, exploded and gushed until the pipeline capped. It took 87 days to cap and seal the ruptured spot on the pipe. A spill of 780,0 00 gallons [10] of crude oil released into the water and spread over 68,000 square miles marking this event as the largest spill in the history. Nearly 5% of the spill cleared by in-situ burning [11] and skimming process.

[2] Photolysis: It is a chemical breakdown of material under the influence of light.

North Dakota pipeline spill [12]: On January 2016, Crude oil spilled at North Dakota from a pipeline. It's said leakage was for a long time and not noticed. After an investigation, it's realized that spill is because of leakage in a pipeline carrying crude oil. Around 18,600 gallons of oil reported leaked on land and causing severe problems in the cleanup.

Refugio County, Texas [13]: In 1997, crude oil of 42,000 gallons spilled and resulted in affecting 11 acres. For the clean-up, In-situ burning method considered for faster clean-up. Fire officials started the burn process in the area of 5-6 acres, and it continued to burn for around 4-5hours continuously. (Figure 1) Shows the in-situ burning in Refugio County, Texas. It's estimated about 90% of oil burned with the help of ISB process [14].

Figure 1: In-situ burning at Refugio County, Texas [15]

Chiltpin Creek, Texas: In 1992, oil spilled from an underground pipeline resulting in 124,000 gallons of crude oil and spread over 38 acres of high marsh area. For clean-up, vacuum trucks used for first four days to collect the oil. Oil penetrated deeper into the marsh area[16] and the spill area burned for faster clean-up. Around 85% of crude oil continuously burned 21 hours. Later the remaining spill area cleaned using other recovery methods. (Figure 2) shows the ISB at Chiltpin Creek, Texas.

Figure 2: In-situ burning at Chiltpin Creek, Texas [15]

List of crude oil spills:

Table 1: List of major crude oil spills [17]

Name	Location	Amount in tones	Year
Deepwater Horizon (Gov't High Est)	The Gulf of Mexico	780,000	2010
Lakeview Gusher	The United States, Kern County, California	1,227,600	1909
Gulf War oil spill	Persian Gulf, Kuwait	1,091,405	1991
IXTOC I	Mexico, Gulf of Mexico	470,000	1979
Atlantic Empress	Off Tobago West Indies	287,000	1979
Fergana Valley	Uzbekistan	285,000	1992
Nowruz Oil Field	Persian Gulf, Iran	260,000	1983
ABT Summer	700 nautical miles off Angola	260,000	1991
Castillo de Bellver	Off Saldanha Bay	252,000	1983

	South Africa		
Amoco Cadiz	Brittany, France	223,000	1978
Amoco Haven tanker disaster	The Mediterranean Sea near Genoa, Italy	144,000	1991
Production well D-103	800 km southeast of Tripoli, Libya	142,860	1980
ODYSSEY	700 nautical miles off Nova Scotia Canada	132,000	1988
Torrey Canyon	Isles of Scilly, England	119,000	1967
Sea Star	The Gulf of Oman	115,000	1972
Texaco Denmark	North Sea, Belgium	107,140	1971
Shuaiba Petroleum Tank	Shuaiba, Kuwait	106,120	1981
Kharyaga-Usinsk Pipeline Spill	Usinsk in Northern Russia (Komi Republic)	104,420	1994
Urquiola	La Coruña, Spain	100,000	1976
Irenes Serenade	Navarino Bay Greece	100,000	1980
Pipeline No. 126 well and pipeline	Ahvazin, Iran	95,240	1978
Hawaiian Patriot	300 nautical miles off Honolulu	95,000	1977
Independenta	Istanbul, Turkey	95,000	1979
Jakob Maersk	Leixoes, Portugal	88,000	1975
M/V Braer	Shetland Islands UK	85,000	1993
Storage tank #6	Forcados, Nigeria	81,290	1979

1.3.2 Clean-up methods for crude oil spill

There are various methods of cleaning oil spills; it depends on the spill location, quantity of spill and other environmental impacts. Some of the clean-up methods of crude oil spills are discussed in the following paragraphs:

Mechanical method:

Many people often use this method during the oil spill. It is a physical or mechanical way of cleaning the oil spills. Shovels and other machinery are used to clean the onshore crude oil spill. The spill is manually shoveled and filled in a container and transported. (Figure 3) shows the manual cleanup method using shovels and other machinery. These spills are manually shoveled and contained in other small containers. Machinery

is used to collect the contaminated spills inside water. Machinery is also used to speed up the clean-up process.

Figure 3: Manual cleanup method using shovel and other machinery [18]

a. Booms: Booms are used to holding the oil at the spill location. Booms are the floating materials placed around the spilled area. Booms are classified into three parts: a ‘freeboard’ or part that rises above the water surface and holds the oil and prevents it from splashing over-the-top, a ‘skirt’ that rides below the surface and prevents the oil from being pushed under the booms and escaping, and a chain that connects the boom. Connected sections of the boom are placed around the oil spill until it is surrounded and contained. (***Figure 4***) Shows the use of boom in containing the crude oil spills. These booms are mainly used in containing oil spills on water.

Figure 4: Crude oil spill clean-up using boom

b. Skimmers: Skimmers are the devices used to collect contained oil using booms. Skimmers can be a sponge, a vacuum device, ships or any other device used to collect the oil. Even the oil attracting materials used to collect spilled oil can also be called as skimmers. Skimmers have limits in obtaining oils; it cannot be used when tidal waves are high. Skimmers are usually used on a still water or still surface. (Figure 5) shows the skimmer used in oil spill recovery.

Figure 5: Clean up using skimmers [19]

c. Sorbents: Sorbents are the materials used to soak oils either by adsorption or by absorption. Oil coats the materials and forms a liquid layer on the surface. Once the layer is formed, it is mechanically removed. In this process, the liquid layer is heavier than water and sinks to the bottom of the sea.

Chemical methods: Usually dispersants are used in cleaning up of oil spills in this method. Dispersants break down the oil into smaller droplets and gets mixed with water. (*Figure 6*) shows the use of dispersants in cleaning the oil spilled area where a man is spraying the dispersant on the crude oil.

Figure 6: Oil spill clean-up using chemical dispersants [20]

Biological method:

Bioremediation: The use of microorganisms to destroy, or reduce the concentration of hazardous wastes on a contaminated site is called bioremediation. This is a natural clean-up process for crude oil spills. Bacteria and fungi are used in breaking down the compound mixture. It's a slow process as it takes years for microorganisms to clean. Bioremediation process is much cheaper and minimal in site disruption. Fertilizers are used in increasing the microorganisms during clean up. (***Figure 7***) Shows the biodegradation process at an oil spilled site. Fertilizers and biomaterials are sprayed at the spilled locations.

Figure 7: Biodegradation method of oil spill clean-up [21]

In-situ burning: In-situ burning means the controlled burning of oil “in place”. In-situ burning requires less labor than most other techniques and can be applied in areas where other methods cannot be used because of limited access to the spill location or ice conditions. In-situ burning method is performed immediately after the spill, a minimum oil thickness of 3mm should be present for the burn to start. Fire resistant booms are used to contain oil spill area during the burn process. In-situ burns have typically removed over 90% of the contained oil during experiments and accidental burns of petroleum on water. The small percentage of the original oil volume left unburned is typically a viscous, taffy-like material that floats for a long enough period of time to be manually removed. Therefore the in-situ method is the most successful method for clean-up. (Figure 8) shows the in-situ burning for an oil spill on sea water. A

fire resistant boom is used to contain the oil spill and fuel is ignited. An intense flame and smoke can be seen during the burn process.

Figure 8: In-situ burning of crude oil spill [22]

1.3.3 *In situ* burning of crude oil spills on sand:

In 1976, Tehran Ltd conducted a study to clean contaminated beach by burning off spilled oil. They considered 11 different methods to burn spilled oils. They are a Fluidized bed, Rotary Klin, Multiple Hearth, Open pit, Pyrolysis chamber, Grate hearth, Retort Furnace, atomized suspension furnace, rotary hearth, shape furnace and inclined hearth. After performing preliminary studies, they considered only 5 among them; they are a Fluidized bed, multiple hearths, grate hearth, rotary hearth. Fuel mixture of 73% sand, 15% crude oil, 12% moisture all by weight considered. After the early test, Rotary Klin method suited for further study as it gave better results compared to the other

device. Using Rotary Klin, tests performed with different sand size; used concrete sand and brick sand (similar to beach sand). Some of the other parameters varied during the test were oil content (15%, 10.6%, 11%, 8%), water content (4%, 6.6%, 7.5%, 11%, 14%) and feed rate (327.6, 166.3, 478.8, 351.1, 252). This setup preheated to a temperature of 925℃ for 6 to 10hours. An only single experiment performed each day and the mixture burned for 2-3 hours. The conclusion shows that this particular method is faster to clean up oiled-sand area [23].

In 1986, Bennett Environmental Consultants Ltd developed a burner with an open-bottomed combustion chamber fitted with skirts. Energy produced from the burner delivered to the positioned clean up area. Diesel fuel used for experiments because of its availability. The quantity of fuel supplied could be adjustable using the nozzle present for feeding. A test site of 6m long and 0.5m wide simulated beach set up. Sand grain size varied from finer ($250\mu m$) to 2.5cm. Waste oil and emulsified oils used during the test. An average efficiency of 76% found from the test conducted. Heat not able to penetrate deeper for continued burning [24].

In 2000 (William et.al,) conducted a series of experiments to find the impact of the intentional burning of oil spilled on wetland environment. They listed some of the main influencing causes during the burn process, some of them are to be plant species, fuel type, and water content with oil, soil type, and burn duration. A test pan of diameter 6m taken for burning test. Five different diesel fuel and six crude oil burns performed. Duration of the test limited to 700s. Thermocouples placed at (0, 0.5, 1, 2, 3, 5, 7 and 10cm) inside the soil. Many different plants planted in the soil at different root depth. Plants usually placed at 30cm depth from the surface of the soil. A hundred and eighty-four specimens of plants exposed to chemical and thermal insult. The soil temperature showed that 10cm of water over the surface of soil helps in preventing damage to plants. A layer of water, just 2 cm below the surface provided a thermal boundary to limit the peak temperatures to 70 ℃. It's showed that heat not penetrated till the depth of the soil as water itself acts as a thermal insulator. Due to this plants recovery and regrowth is possible as the roots do not reach a temperature above 60℃. Burning with diesel fuel showed a higher heat flux on the surface of the fuel. The soil temperatures

were the same compared with crude oil burning. Plants placed at a height of 2cm achieved temperatures more than 70 ℃ and showed they can never be grown again [25].

Various experimental approaches proposed in finding a better in-situ method to clean the contaminated oil sands. One such effort is “Experimental and simulation study of *in situ* combustion process in carbonate fractured porous media”[26, 27]. Working principle of Toe to Heel air injection (THAI) [28] method is used. This integrates both in-situ combustion and advanced horizontal well method. In this, carbonate rocks are powdered and separated to different grain size. The mixture is then mixed with two different API’s of crude oil. Fresh oxygen supplied from the top to support combustion. Thermocouples placed at the center with 5cm apart; igniter placed at the top of the furnace to ignite the mixture at a certain temperature. Sand and crude oil mixed according to the following equation: $\frac{m_0}{m_s} = \frac{\rho_0 \emptyset s_0}{\rho_s(1-\emptyset)}$. Combustion started at the temperature of 573-673K. Percentage of CO_2, CO and recovery of combustion tube test found to be around 30%- 45%, 15% - 20% and 71% - 52.16% respectively. The error range between experimental and simulation result found to be 10.322% and 11.21% for CO_2 and cumulative oil recovery respectively. Error percentage for CO release from effluent gas was the same. From this experiments grain size and air injection rate showed a significant change in achieving maximum recovery.

Pironi [29], in his thesis dissertation for Doctor of Philosophy, has conducted research on “Smouldering Combustion of Organic Liquids in Porous Media for Remediating NAPL-contaminated Soils”. In this study, he performed various laboratory experiments to find the potential of smoldering combustion for Non-aqueous phase liquids (NAPLs). Smoldering combustion is a flameless burning of a condensed fuel that drives heat from surface oxidation reactions[30], Small scale (~15cm) and Intermediate scale experiments (~30cm) are performed. Air flow of 2.29, 4.75, 7.94 and 16.2 cm^3/s injected through air diffuser inside the furnace. Fuel ignites and continues to burn, and then air supply is stopped. Crude oil with saturation between 10% - 50% has been used. Furnace preheated for 50min till it reaches a temperature of 400℃. Thermocouples

mounted on a holder and placed at the center of the furnace to measure the temperature distribution along contaminated sand during smouldering process.

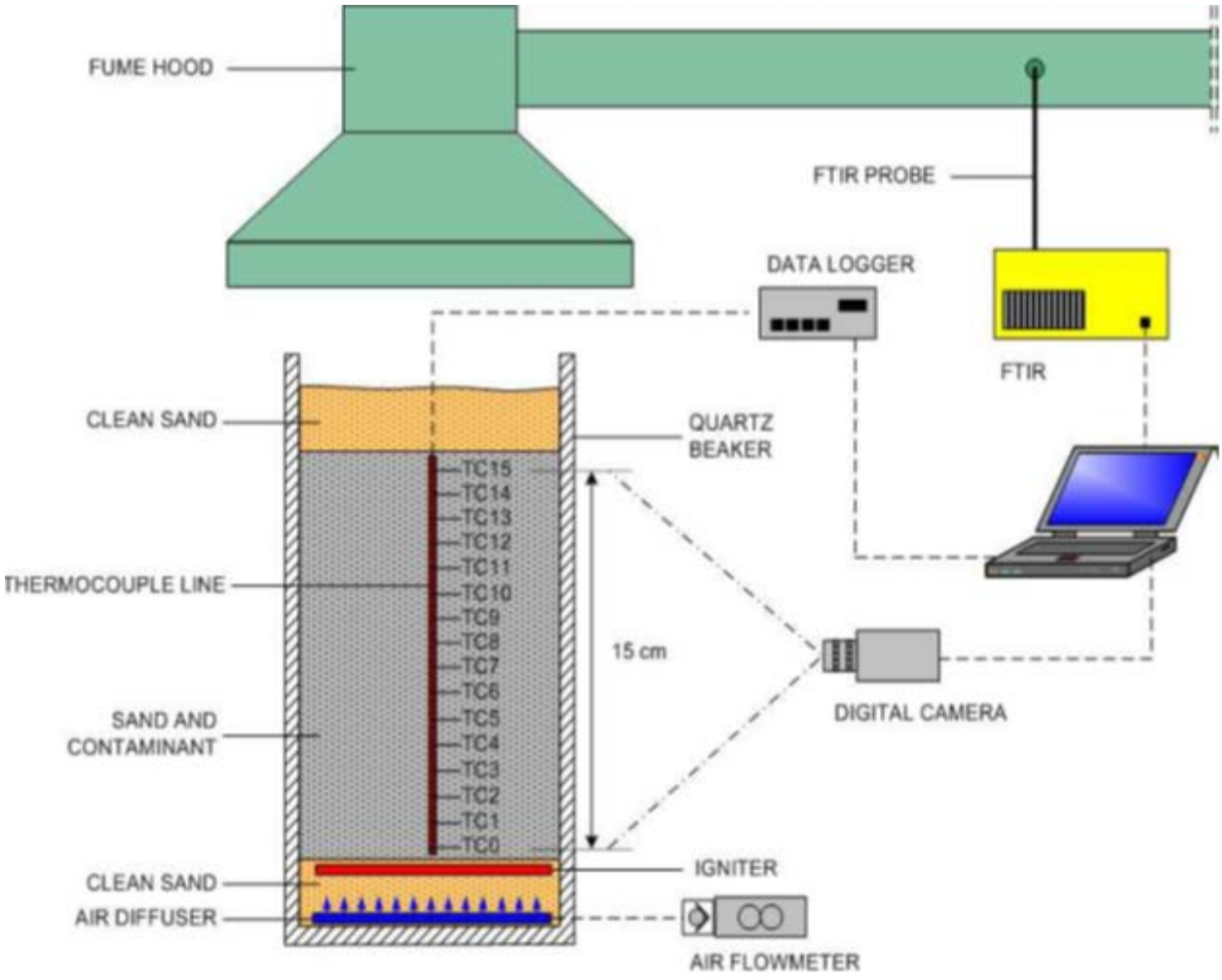

Figure 9: Schematic diagram of small scale apparatus for smoldering process [31]

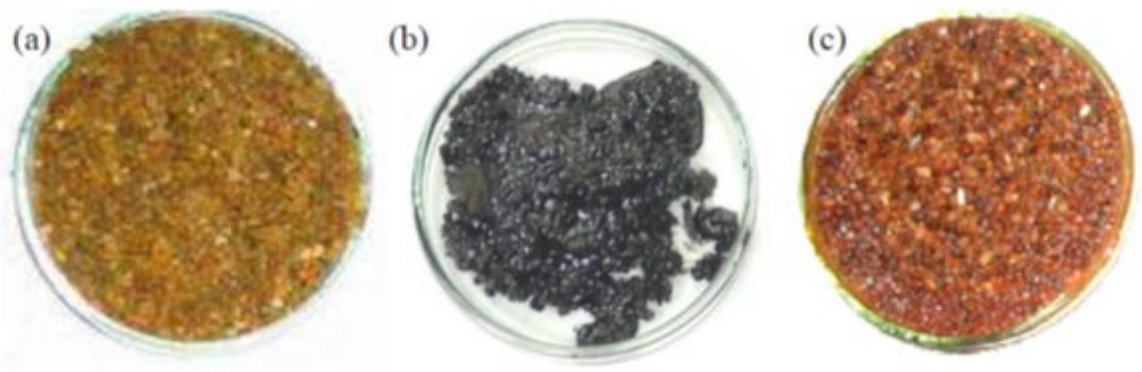

Figure 10: (a) before mixing with coal tar (b) after mixing with coal tar and (c) after smoldering [31]

Small scale experiments with organic liquids embedded within oil matrix can successfully smolder. In intermediate level, detailed behavior of the combustion process including its relationship to mass and energy balance and the evolution of temperature profiles. It shows smoldering process is self-sustaining and self-terminating. The 30 column sensitivity experiments demonstrated a broad range of process parameters - including contaminant type, contaminant mass, soil type, and oxidizer flow rates. From the results, it also showed a contaminant mass removal of 99.5%. Maximum burning temperatures observed in the range 600-1100 ˚C. Average propagation velocities varied between $0.7e-04$ and 1.2e-04 m/s. Intensity and velocity of process shows to control by the rate at which oxidizer delivers. Contaminant type and mass noted to affect peak temperatures and propagation velocity, influencing the energy balance at the reaction front.

Chapter 2

2.1 Methodology

An experimental approach consisting of observations and measurements was used to conduct this research. A detailed description of experimental design and parameters related to this study is provided in this chapter.

2.2 Experimental Setup

The cone calorimeter is often used as a bench scale instrument in fire testing [32]. It derives its name from the conical shape of the heater[33]. As shown in Fig. 11 the cone calorimeter comprises a cone heater, igniter, sample holder, gas analyzer, hood, and load cell. Experiments are performed by exposing the surface of a sample to a uniform radiative heat flux from the cone heater and characterizing flammability parameters such as time to ignition, mass burning rate, O2 consumption, CO/CO2 production, and soot yield. For the current study, a new sample holder capable of holding a mixture of sand and oil was designed and constructed.

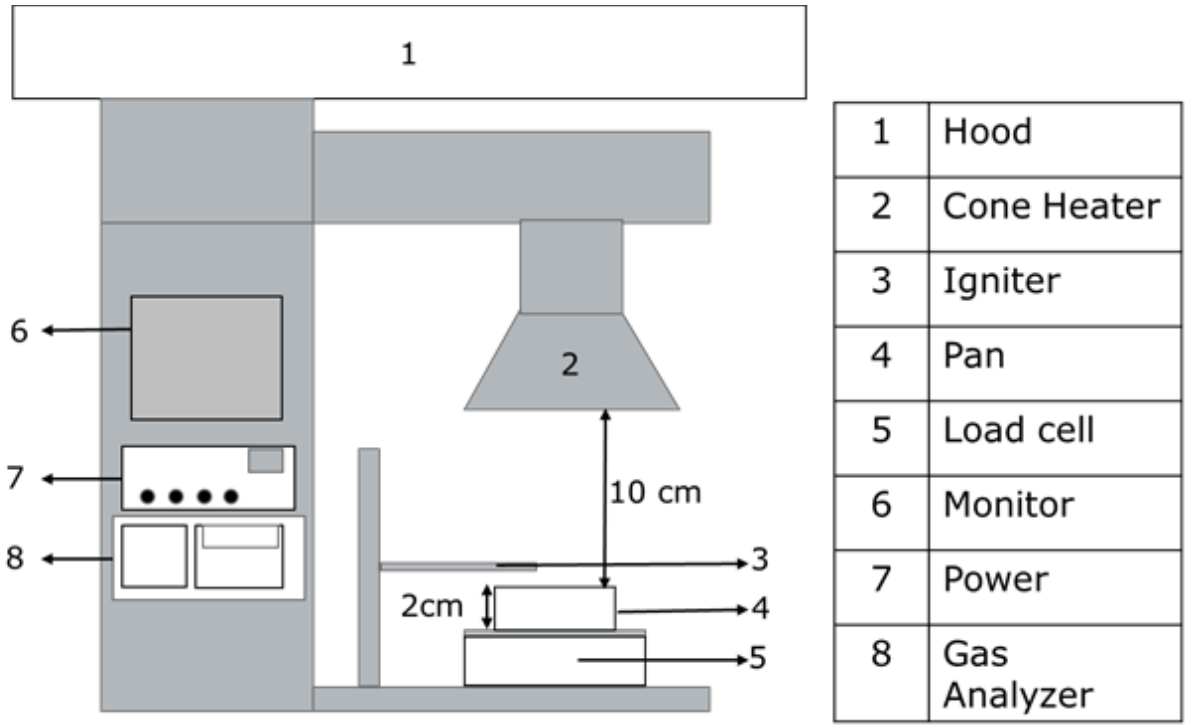

1	Hood
2	Cone Heater
3	Igniter
4	Pan
5	Load cell
6	Monitor
7	Power
8	Gas Analyzer

Figure 11: Experimental setup

All the experiments are performed in steel pan of 10cm diameter and 2cm height. Steel pan is insulated with a thickness of 1cm around the circumference. Pan is placed on a heat resistant sheet of 1cm thickness, which is placed on load cell (Sartorius “ED6202S-CW” precision of 0.01g and 5 data points collected for every second) to measure the change in mass during the test. The entire setup is placed under a high capacity hood for the smoke to escape.

The test procedure comprised of placing the test specimen at a distance of 10cm below cone heater. Uniform radiant heat flux is applied to fuel surface. Spark igniter placed at a distance of 1cm above the fuel surface and 9cm below the cone heater. Igniter starts immediately after opening the shutter of the cone heater. Igniter ignites the flammable gasses passing from the fuel surface. The igniter is turned off immediately after the flame appears. A fan is mounted at the end of the hood to monitor the flow rate of combustion products. Flue gasses are passed through the hood situated right above the cone heater.

Alaskan North Scope (ANS) crude oil is used in preparing emulsions. Crude oil is a mixture of hydrocarbons with different molecular weights. It behaves transient as some of its properties differ with time. Table 2 shows properties of ANS crude oil [34].

Table 2: ANS Crude oil properties [34]

Density ($\frac{kg}{m^3}$)	868.6
Viscosity (centi-poise, cP)	-6.7-32.3
Boiling point (℃)	38-570
Thermal conductivity K ($\frac{W}{m\,K}$)	0.132
Specific heat capacity, C_p($\frac{kJ}{Kg\ K}$)	2.3
Latent heat L_v($\frac{kJ}{kg}$)	250

Fuel used in all the experiments is a mixture of sand and crude oil emulsion. An emulsion is prepared by mixing 60% salt water and 40% ANS crude oil in a blender of 1litre capacity and blended at low speed for around 1 hour and 30 minutes. The emulsion is then air cooled for some time to check for its stability before mixing with sand. If the emulsion is stable, then it is mixed with sand if not it is again blended for 30 – 45 minutes. (Figure 12) Shows the emulsion percentage in a beaker. Sand of porosity 37% - 40% is used in all the experiments.

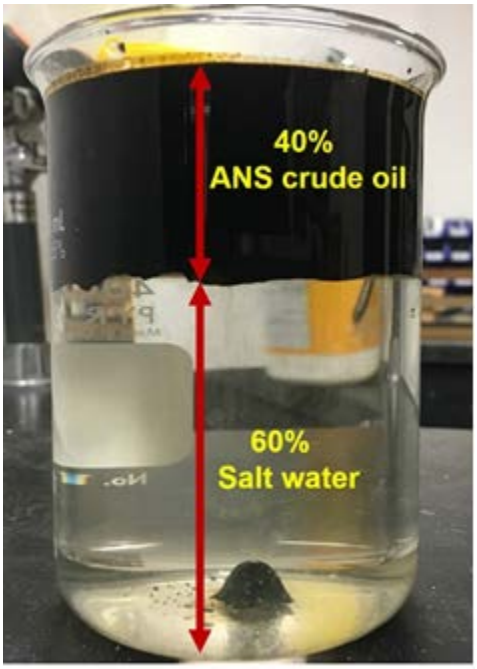

Figure 12: Before Emulsification

Emulsion and sand are mixed in two different percentages having 18% and 24% of the emulsion. Lower emulsion content – Fuel-sand mixture is prepared by mixing 18% emulsion and 82% sand by mass and in higher emulsion content - 24% emulsion and 76% sand are mixed.

A water cooled heat flux gauge is placed under the cone heater [32] at a distance of 10cm. Cone heater is set to a different temperature that gives required heat flux. Figure (13) shows the calibration curve for temperature (℃) with respect to heat flux ($\frac{kW}{m^2}$). With this curve, a given temperature is set to obtain the required heat flux from cone heater during the experiment.

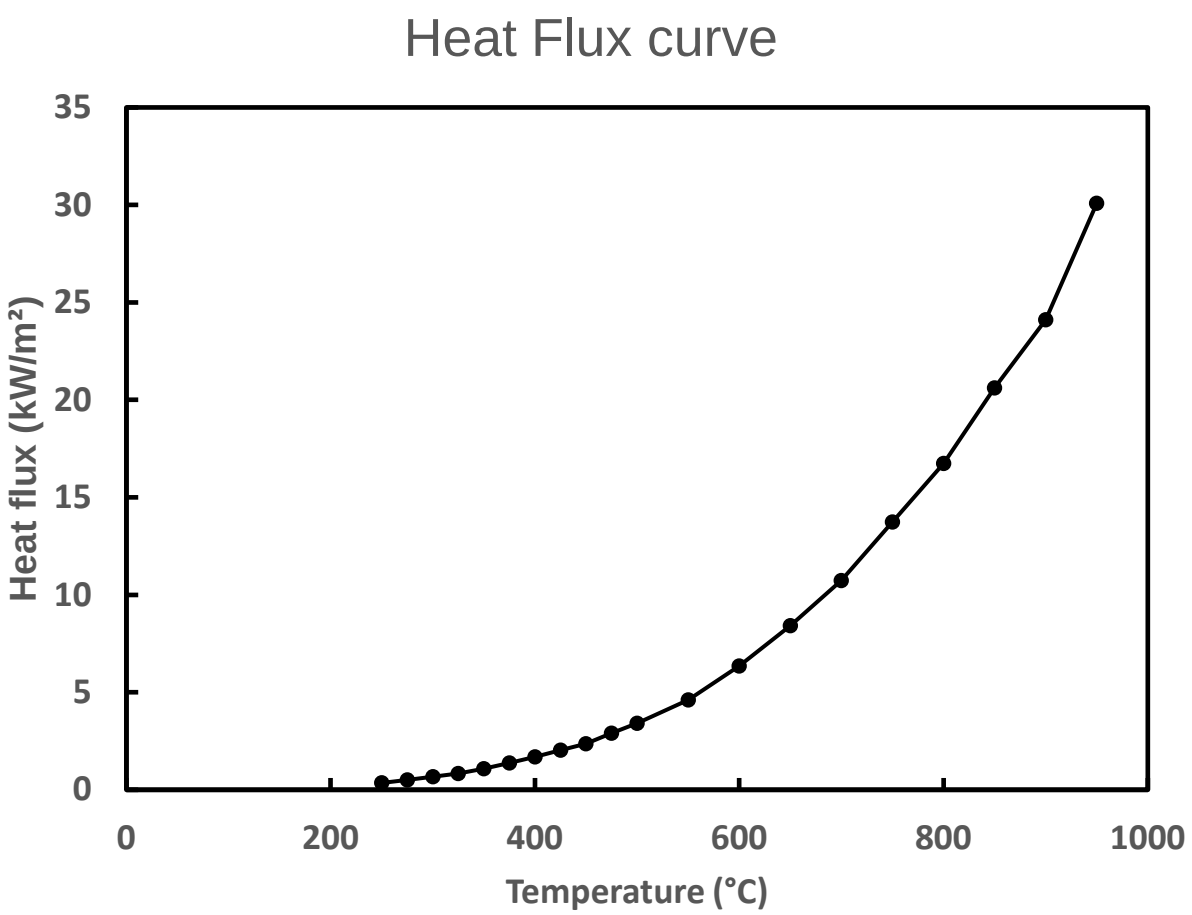

Figure 13: Cone heater Calibration curve

2.2.2 Experimental matrix

A flow chart of the experimental matrix is shown in Fig 14, all the experiments have been repeated for three times. Copper rod of diameter-1cm is used in all the experiments performed. For multiple rods highlighted with superscript * diameter of both 1cm and 0.45cm have been used to perform experiments.

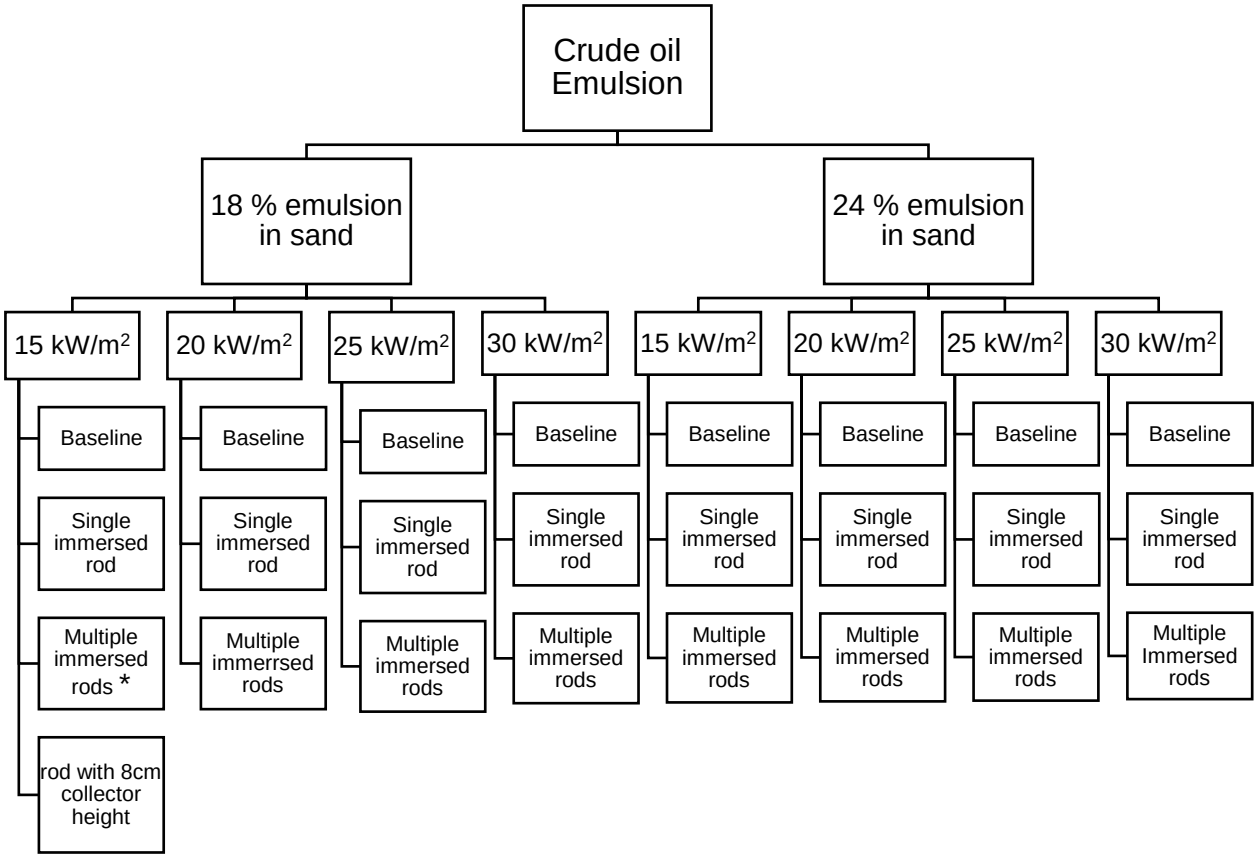

Figure 14: Experimental Matrix

2.2.3 Baseline cases

The fuel mixture of sand and crude oil emulsion are mixed and poured into the test pan up to a height of 2cm. Total of six K-type thermocouples are placed in the test pan to measure the temperature variations at those with a separation distance of 0.8cm from each other and are placed inside the fuel bed at the center. Other 3 thermocouples are placed at the inner wall of the pan, the outer wall of the pan and outside the insulated material as shown in Fig 15. The mass sample size of the mixture is around 200g for the baseline cases.

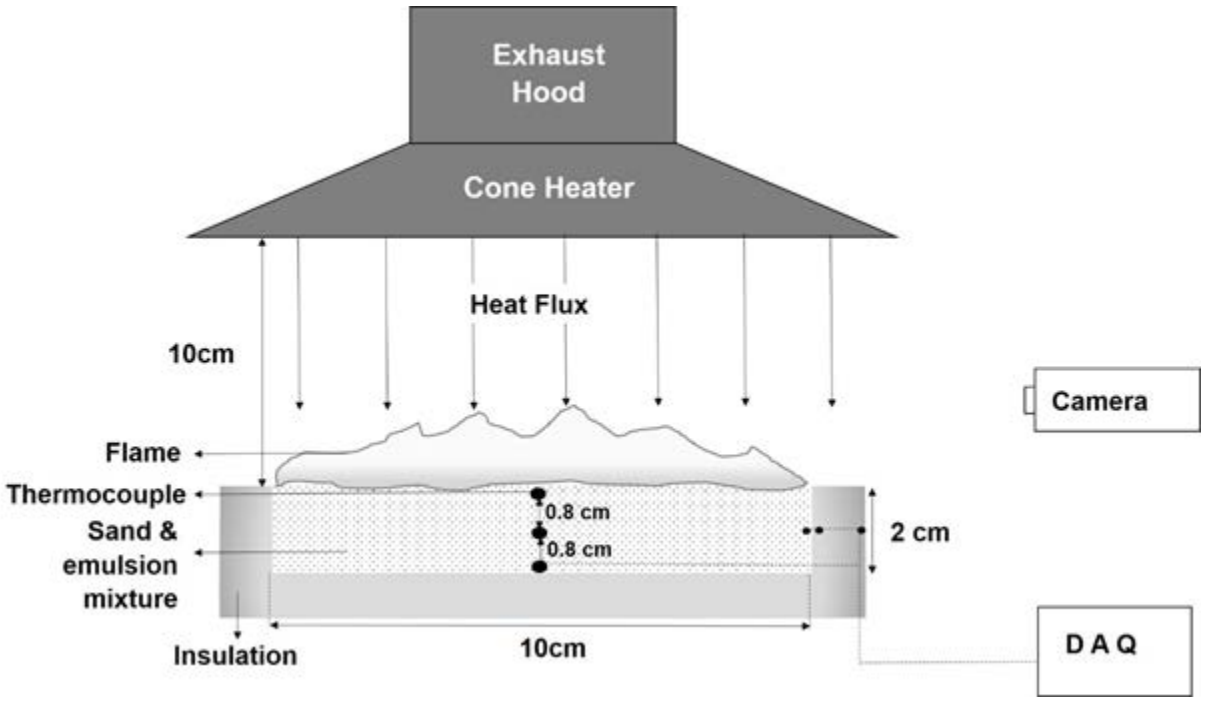

Figure 15: Baseline test setup

2.2.4 Cases with single immersed rod

Highly conductive copper rod (k=385$\frac{W}{m\,K}$) of 2cm height and 1cm diameter is immersed at the center of fuel mixture. Total of 9 thermocouples are used to measure temperature distribution during the test. Three thermocouples are placed partially inside the copper rod and 3 more are mounted on thin ceramic tube and placed 1cm offset to the copper rod, thermocouples are placed separated by 0.8 cm from each other. Other 3 thermocouples are placed at the inner wall of pan, outer wall of pan and outside the insulation wall. (Figure 16) shows the sketch of single copper rod immersed inside the fuel mixture as well the thermocouples placed. A mixture having mass around 200g is used for all the cases with single immersed rod case.

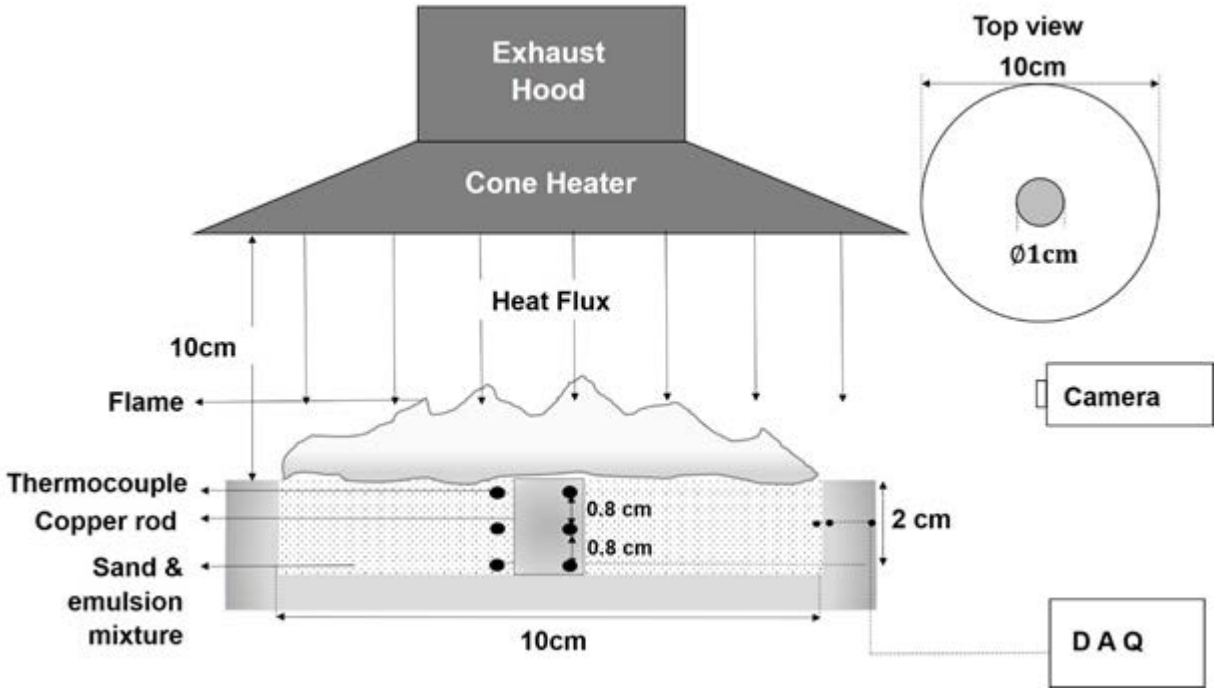

Figure 16: Single immersed rod setup

2.2.5 Cases with multiple immersed rods

Five similar copper rods of 2cm height and 1cm diameter are placed inside the fuel bed separated by 2cm from the center rod. The arrangement of rods and placement of thermocouples are shown in Fig 17. Total of 9 thermocouples are used to measure temperature distribution during the test conducted. The arrangement of thermocouples is same as that in the single immerses rod cases. However, in this case, around 190g of the fuel mixture is used in all the experiments. In order to maintain the same porosity of the fuel mixture with another case, the mass of the fuel mixture has been reduced. This has been calculated by subtracting the volume of the rods immersed with the volume occupied in the baseline case. In the baseline case, the volume of pan is 157cm^3 which can hold around 200g of fuel mixture. When 5 copper rods of diameter 1cm are immersed inside the pan, the available volume in the pan is 149.23 cm^3 and can hold a fuel of 190 g.

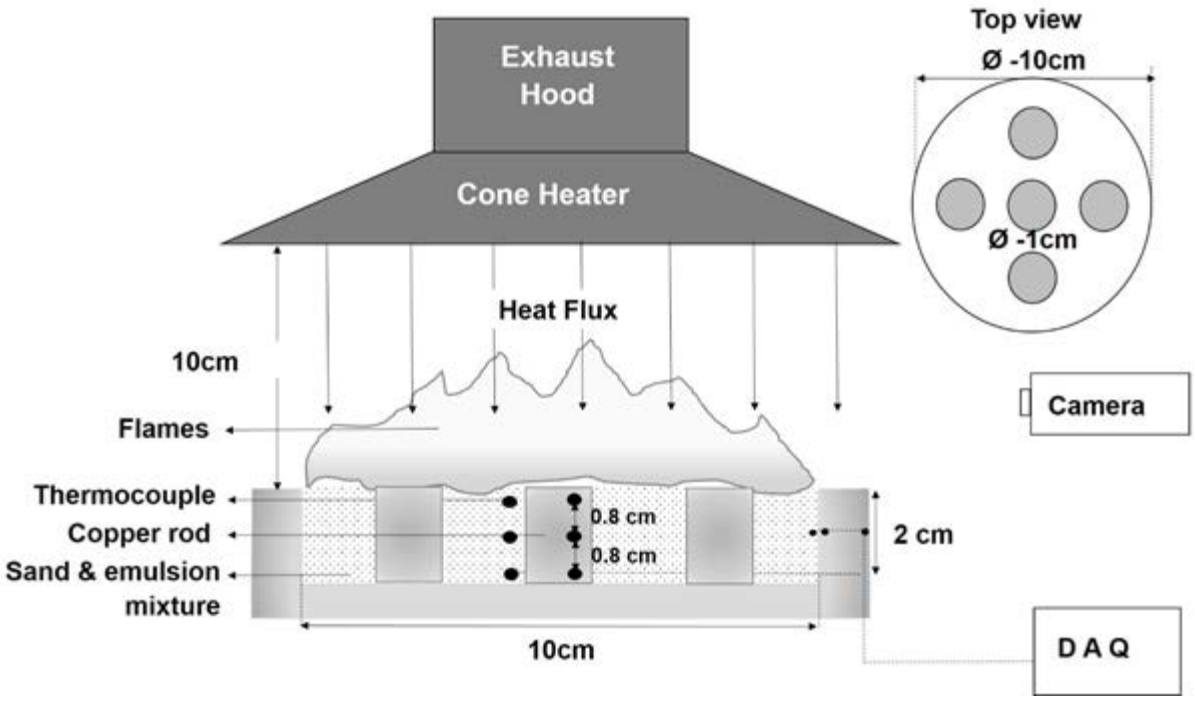

Figure 17: Multiple Immersed rods - test setup

2.2.6 Cases with higher rod height and lower rod diameter

Copper rod of 10cm is placed at the center of the fuel mixture as shown in Fig 18. The portion having 8cm length is in contact with the flame to receive its heat flux and acts as a heat collector. The remaining 2cm portion is immersed in the fuel mixture and acts as a heater. Heat is conducted on the top surface of the rod and conducted through it to heat the fuel mixture. Thermocouples are placed similarly to the positions as in the case of single immersed single rod.

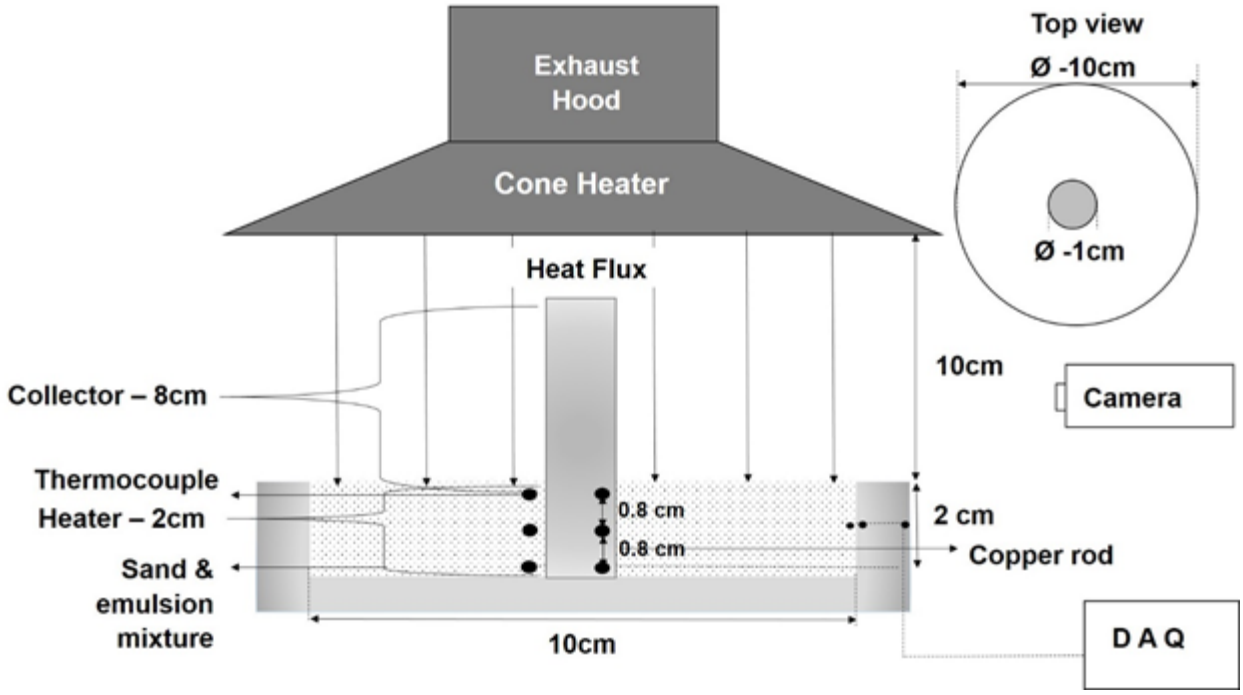

Figure 18: Increased height of rod test setup

In another configuration, five similar copper rods each of 2cm height and 0.45 cm diameter are placed inside the fuel bed separated by 2.5cm away from the center rod. The arrangement of rods and placement of thermocouples are shown in Fig 19. Thermocouples are placed in a similar way as in the case of immersed copper rod. Summation of surface area (a copper rod with diameter 0.45cm) exposed to the heat flux is equal to the surface area in the case with the single copper rod as shown in Fig 16. Equation (1) shows the area exposed to heat flux by each rod and Equation (2) shows the areas exposed to heat flux are equal. Whereas the surface area available inside the fuel (heater part) is greater in the case with 5 smaller rods as compared with the surface area of the single copper rod.

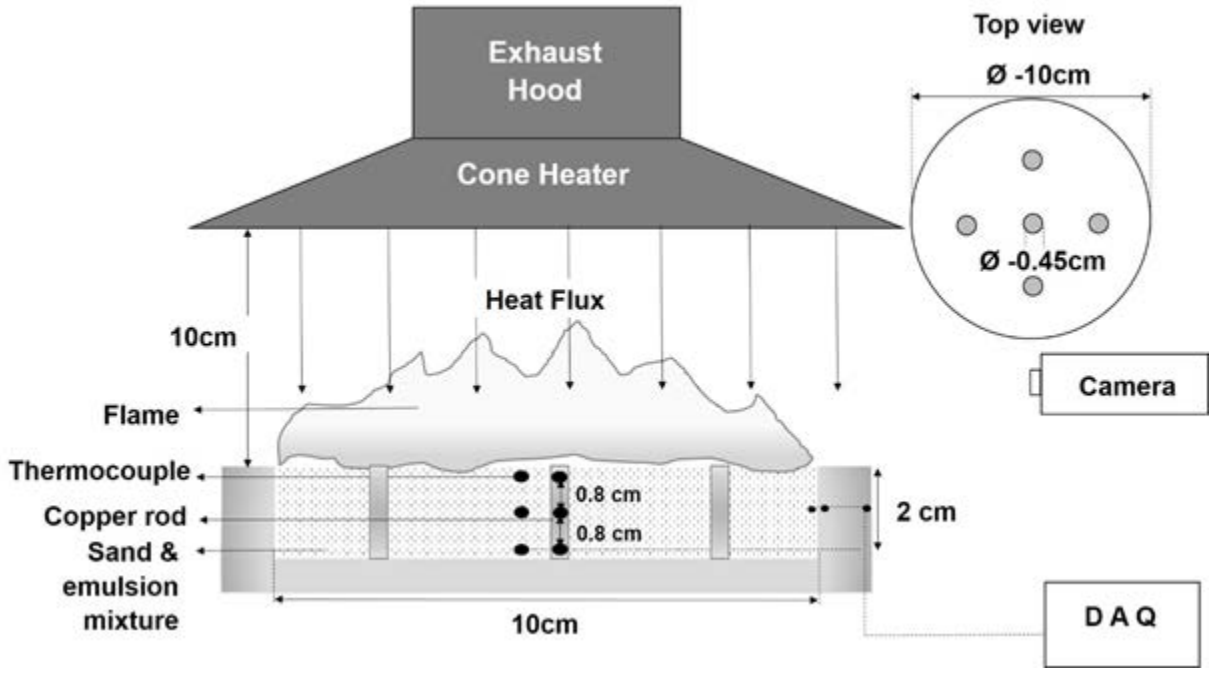

Figure 19: Test setup for multiple immersed rods (Ø-0.45cm)

Chapter 3

3.1 Results

As discussed, the emulsion-sand mixture having emulsion percentage in the range of 18% to 24% is considered in this study. The mixture is subjected to four different heat flux values (15, 20, 25, and 30$\frac{k\,W}{m^2}$) in order to study the ignition time, combustion and heat transfer to the mixture. During the experiment, external heat flux from cone heater uniformly heats up the surface of fuel. Spark igniter is turned on immediately after the shutter of the cone heater is opened. As the mixture heats up, water present in emulsion separates and evaporates. Crude oil present in the mixture also gets heated up and when its temperature crosses the flash point, enough vapors are available at the surface. Based on the temperature of the sand layer, fuel vapors are present within the porous bed as well. After enough volume of flammable mixture becomes available at the surface, the ignition source causes ignition and a flame is formed over the porous bed. If enough oxygen penetrates into the pores, then smoldering combustion may also be present within the porous mixture. Time taken for a flame to form over the surface is known as ignition time for the given mixture in the given configuration.

3.1.1 Ignition time

As the surface heats up to a sufficient temperature, ignition onsets, and a flame appears over the surface. Based on the surface temperature, flashes appear, which indicate occurrences of instantaneous premixed flames and subsequently steady flame sustains. Ignition time changes depending upon fuel composition, primarily on the quantity of crude oil present in the mixture. For baseline experiments, with the exception of 18% emulsion case at 15 kW/m^2 heat flux, all mixtures ignited at all input heat flux values. Only flameless, smoky process was observed in the 18% emulsion case at 15 kW/m^2.

For this case, when a single copper rod (1cm diameter) is immersed till the height of fuel bed at the center, ignition occurred in around 540 *s* and flashes of flames have been observed. However, sustained diffusion flame has not been seen. This improvement is due to the heat transferred by the copper rod to the interior of the bed allowing increased amount of fuel vapors to escape to the surface. For the same case, when multiple fuel configurations as shown in Fig. 19 was used, ignition occurred in around 340 *s*, and this time a steady diffusion flame has also been observed. (Tables 3 and 4) report the ignition time (in seconds) for all the cases. Values reported are averaged using the data from three repeated trials. Values for all the trials are reported in Appendix A.

Table 3: Ignition time for fuel mixture (18% of emulsion & 82% sand)

Heat flux ($\frac{kW}{m^2}$)	**Baseline (s)**	**Single immersed rod (s)**	**Multiple immersed rods (s)**
15	no flame	540	340
20	240	180	178
25	150	110	108
30	136	85	85

Table 4: Ignition time for fuel mixture (24% of emulsion & 76% sand)

Heat flux ($\frac{kW}{m^2}$)	**Baseline (s)**	**Single immersed rod (s)**	**Multiple immersed rods (s)**
15	470	430	424
20	383	320	318
25	317	240	230
30	288	180	180

Fuel ignited faster when compared with baseline test due to the enhanced heat transfer from the immersed rods. However, for higher heat flux cases and for a higher percent of the emulsion in the mixture, cases with multiple rods have not shown any significant

change in the ignition time as compared to the case with single immersed rod. From Tables 3 and 4, it can be seen that, for the same heat flux, ignition time increases with increase in the quantity of emulsion in the mixture. As the quantity of emulsion increased, the quantity of water also increased which makes hard for the fuel to ignite.

3.1.2 Mass loss

Mass loss of fuel is measured by a load cell, placed below the test pan. Fuel-sand mixture of the initial mass of around 200 g is taken for the cases of baseline and single immersed rod. For the cases of multiple immersed rods, an initial mass of 190 g is taken. Table 5 shows the distribution of the sand and emulsion in the mixture in 200 g case and Table 6 shows the same for 190 g mixture.

Table 5: 200g fuel composition

Material	**Mass (g)**	
	Case a [3]	**Case b** [4]
Dry sand	164 g	152 g
Water in oil emulsion	36 g	48 g
	Saltwater: 21.6 g	Saltwater: 28.8 g
	ANS Crude oil: 14.4 g	ANS Crude oil: 19.2 g

[3] case a: 18% of emulsion and 82% of sand

[4] case b: 24% of emulsion and 76% of sand

Table 6: 190g fuel composition

Material	Mass (g)	
	Case a	Case b
Dry sand	155.8 g	144.4 g
Water in oil emulsion	34.2 g	45.6 g
	Salt water: 20.52 g	Saltwater: 27.36 g
	ANS Crude oil: 13.68 g	ANS Crude oil: 18.24 g

Table 7 shows the total mass loss of the fuel and time at which the flames self-extinguished during the test for 18% of emulsion and 82% of sand [case (a)]. A complete combustion has not been observed for the baseline tests, especially at 15 kW/m^2. In baseline case at 15 $\left(\frac{kW}{m^2}\right)$ heat flux, flames are not seen during the experiment. At 20 $\left(\frac{kW}{m^2}\right)$ heat flux, fuel ignites and do not burn for long time and self-extinguishes around 530 s. At higher heat fluxes of 25 and 30 $\left(\frac{kW}{m^2}\right)$, fuel burnt with steady flames till the end and finally extinguished.

Table 7: Mass loss of fuel (18% of emulsion with 82% sand)

	Mass loss (g)			Time to extinguish (s)		
Heat Flux $\left(\frac{kW}{m^2}\right)$	**Baseline**	**Single immersed rod**	**Multiple immersed rods**$(\emptyset - 1cm)$	**Baseline**	**Single immersed rod**	**Multiple immersed rods**$(\emptyset - 1cm)$
15	30.6 [*5]	31.56	34.2	1271	828	820
20	21.4	31	34	530	770	770
25	30	36	34.2	650	846	660
30	31	35	34.2	912	687	470

[5] *: No flame were found (Smouldering combustion).

Experiments were conducted till the flame extinction is observed. There are two phases observed during the experiments. The first phase is till the fuel is ignited and a flame anchor over the surface and second phase is the burning of fuel with flame till it extinguishes naturally. At lower heat flux, fuel is not heated enough for continues vaporization and hence results in flame extinction.

Table 8 shows the total mass loss and time at which flame extinguishes, for 24% of emulsion and 76% of sand [case (b)]. At lower heat flux of 15 $\frac{kW}{m^2}$ and 20 $\frac{kW}{m^2}$, a complete combustion is not seen for any of the case (baseline, single immersed rods and multiple immersed rods). Copper rods help in burning more fuel in lesser time, as compared to that of baseline. At higher heat fluxes of 25 $\frac{kW}{m^2}$ and 30$\frac{kW}{m^2}$, 100% of fuel is burnt for all the cases.

Table 8: Mass loss of fuel (24% of emulsion with 76% sand)

	Mass loss (g)			**Time to extinguish (s)**		
Heat Flux ($\frac{kW}{m^2}$)	**Baseline**	**Single immersed rod**	**Multiple immersed rods($\emptyset - 1cm$)**	**Baseline**	**Single immersed rod**	**Multiple immersed rods ($\emptyset - 1cm$)**
15	37	37	40	803	787	1230
20	38	40	42	734	699	1280
25	48	48	45.6	976	893	740
30	48	48	45.6	880	818	668

Moisture content in the fuel can be seen in Figs. 20 and 21. After the fuel burns completely, the solid material is left behind. (Figures 20 and 21) show the photographs of the burnt fuel (24% emulsion and 76% sand) at an incident heat flux of25 $\frac{kW}{m^2}$. Photographs are taken after the fuel is burnt and cooled till the smoke is clear.

Figure 20: Cross-sectional view of burnt fuel at 25 kW/m^2 heat flux

Figure 21: Top view of burnt fuel at 25 kW/m^2 heat flux

Table 9 shows the percentage of fuel emulsion burnt in case (a). This percentage is calculated using the formula:

$$\frac{initial\ mass - mass\ at\ time\ (t)}{total\ mass\ of\ emulsion} * 100$$

At lower heat fluxes of *15* $\frac{\mathrm{kW}}{\mathrm{m}^2}$ *and 20* $\frac{\mathrm{kW}}{\mathrm{m}^2}$*,* copper rods influence in burning the fuel within a limited time. With the single immersed rod, fuel is burnt more when compared with baseline. With multiple rods as well, the fuel is completely burnt; i.e., 100% burning is seen during the test. At higher heat flux of *25* $\frac{\mathrm{kW}}{\mathrm{m}^2}$ and *30* $\frac{\mathrm{kW}}{\mathrm{m}^2}$, almost complete

combustion (97%-100%) is obtained when compared with that of the baseline (83%-86%).

Table 9: Mass loss (%) for case (a)

Heat Flux ($\frac{kW}{m^2}$)	Baseline (%)	Single immersed rod (%)	Multiple immersed rods (%)
15	85[6]	87.6	100
20	59.4	86.1	99.4
25	83.3	97.2	97.95
30	86.1	97.2	100

Table 10 shows the percentage of fuel (emulsion) burnt in the case of 24% of emulsion with 76% of sand (case (b)). At lower heat fluxes of *15* $\frac{\mathrm{kW}}{\mathrm{m}^2}$ *and 20* $\frac{\mathrm{kW}}{\mathrm{m}^2}$*,* influence of immersed copper rods shows an increase in the percentage of fuel burnt, especially with multiple rods. As the emulsion content is increased in the fuel, the water content is also increased and this water restricts the fuel for complete combustion and also the flames are not found to be stable until the end. At the Higher heat flux of *25* $\frac{\mathrm{kW}}{\mathrm{m}^2}$ *and 30* $\frac{\mathrm{kW}}{\mathrm{m}^2}$*,* fuel is completely burnt (100%) for all the three cases (baseline, single immersed rod, and multiple immersed rods.

Table 10: Mass loss (%) for case (b)

Heat Flux ($\frac{kW}{m^2}$)	Baseline (%)	Single immersed rod (%)	Multiple immersed rods (%)
15	77	77	87.7
20	79.1	83.3	92.1

[6] - Fuel burnt without any flame. Fuel is both evaporated and smouldering combustion taken place.

25	100	100	100
30	100	100	100

3.1.3 Temperature profiles

Temperature is measured using thermocouples placed inside the fuel. Placement of these thermocouples is shown in Figs. 16, 17 and 18. Top surface of the fuel start to heat as soon as the shutter of cone heater is opened. Radiative heat flux heats the surface of the fuel till it ignites. After the fuel is ignited (flames) then flames start to heat with the radiative heat flux. In baseline case, fuel is heated only with the applied external heat flux and also with the convective flames. Immersed copper rods having a conductivity of (k = 400 W/mK) heats the fuel with flame heat and radiative heat. The top surface of the copper rod exposed to heat flux acts as a heat collector and the surface inside fuel acts as a heater. In baseline test, heat is not passed till the bottom of the fuel, immersed copper rods heats the fuel entire fuel and increase the burning rate.

To ignite the fuel mixture a certain temperature is to be attained for flames to appear on the surface of the fuel. At the certain time even though required temperature is attained at the surface of the fuel, flammable hydrocarbons will be evaporated. Fuel ignition temperature is shown in the below table for two fuel mixtures at different heat flux. In porous media, the ignition temperature varies widely. An average of the three test is shown in the table below. Detailed values are tabulated in the appendix section. Tables 11 and 12 show the temperature of the fuel surface at ignition (flame). Values are averaged for three tests and in detail, test result is shown in Appendix A.

Table 11: Ignition Temperature for 18% Emulsion and 82% sand (case (a))

Heat Flux ($\frac{kW}{m^2}$)	**Baseline** (℃)	**Single immersed rod**(℃)	**Multiple immersed rods**(℃)
15	No Flame	220	204
20	136	129	150
25	111	97	181
30	95	133	140

Table 12: Ignition Temperature for 24% Emulsion and 76% sand (case (b))

Heat Flux ($\frac{kW}{m^2}$)	**Baseline**(℃)	**Single immersed rod**(℃)	**Multiple immersed rods**(℃)
15	158	164	165
20	138	177	139
25	143	159	166
30	139	148	160

3.1.4 Emissions from fuel mixtures

Along with the measurements of mass loss, temperature profile, CO and CO_2 are measured using the gas analyzers. CO and CO_2 analyzers are placed inside the exhaust hood in line with the oxygen analyzer to determine the combustion chemistry and toxicity. The flue gasses during the burning of fuel mixture sample are collected into the extraction hood situated directly above the heater. A fan is mounted in the exhaust line to set the flow rate of the combustion products[32]. The gas sampler is situated just before the fan in the exhaust line. Before passing through the gas analyzer, smoke is passed through the filters to remove some particles. The smoke measurement system is situated in between the gas analyzer and the fan. Analyzers such as carbon monoxide and carbon dioxide analyzers are usually fitted for a better understanding of burning process[32]. This gas is monitored with the Servomex gas analyzer (Industrial gas analyzer - 4200). The measuring range of this device for CO_2 is 0-10 ppm of CO_2 and for CO it is 0-50 ppm of CO.

Calibration of analyzers before performing experiments is necessary to get accurate results. The gas analyzers are calibrated by using nitrogen gas, CO, and CO_2 gas. For the burning efficiency, C-factor is calibrated with a methane burner. In this, only CO and CO_2 gas analyzers are calibrated. During the calibration process, nitrogen gas is used for calibrating lower value (0%) and the air is used to calibrate the higher values (1% and 2.5% for CO and CO_2 respectively). The combustion products during the experiments are recorded continuously by a data acquisition system.

(Figure 22) shows the CO_2 emission for the fuel mixture of 18% emulsion and 82% sand mixture exposed to a heat flux of $15 \frac{\mathrm{kW}}{\mathrm{m}^2}$. Three different curves are seen in Fig 22, representing the multiple rods, single rod, and baseline test. The plots are fitted to a fourth order polynomial function. From the figure, it is seen that the CO_2 release is higher in the multiple immersed copper rods compared with single immersed rod and baseline tests as the fuel is completely burnt with the multiple immersed rods case. In the baseline case, as there was no flame on the surface of the fuel mixture, there is no change in the curve (dotted line in Fig 22).

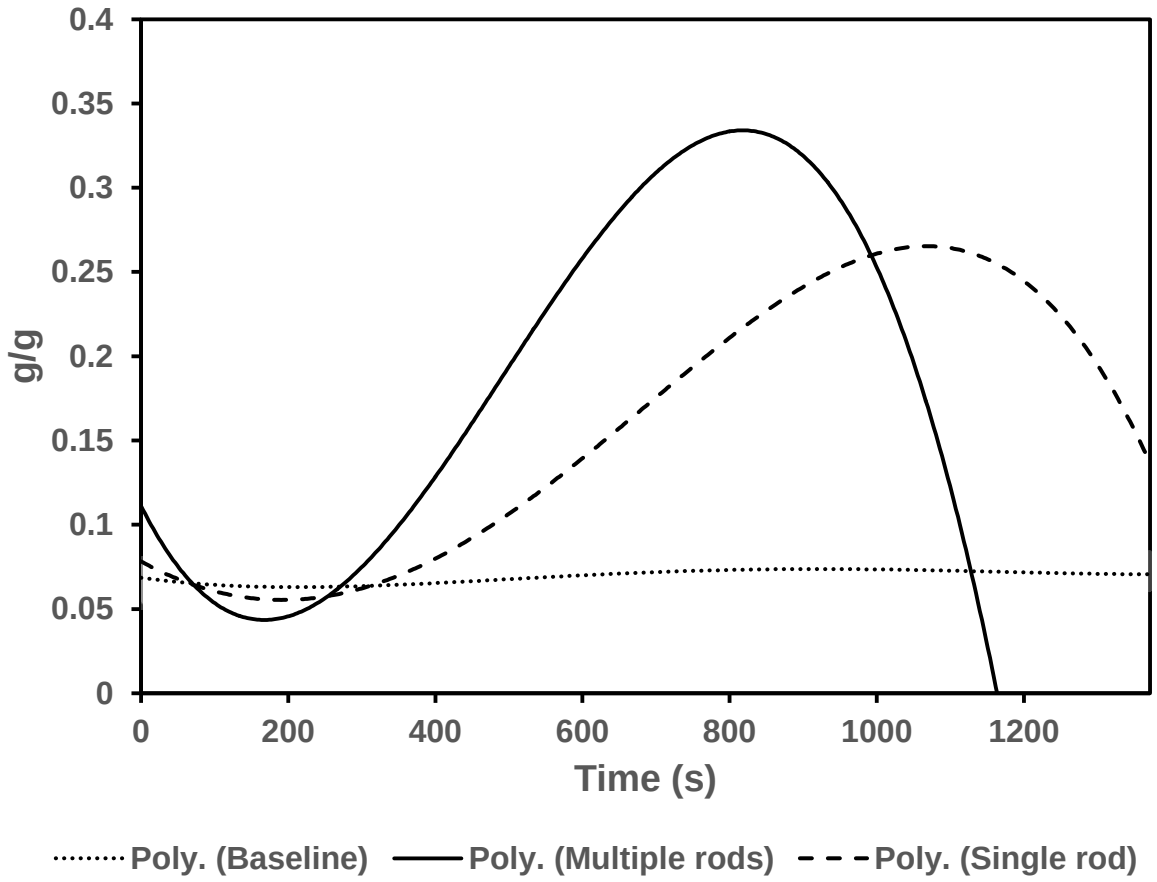

Figure 22: CO_2 emission from 18% emulsion and 82% sand mixture burnt at 15 $\frac{kW}{m^2}$ heat flux

(Figure 23) shows the CO release for the fuel mixture of 18% emulsion and 82% sand mixture exposed to a heat flux of 15 $\frac{kW}{m^2}$. Three different curves are seen in Fig 22, representing the multiple rods, single rod, and baseline test. There is no change in the curves for CO emission during the test, as the sensitivity of the CO analyzer is to less to sense the CO particles in the smoke.

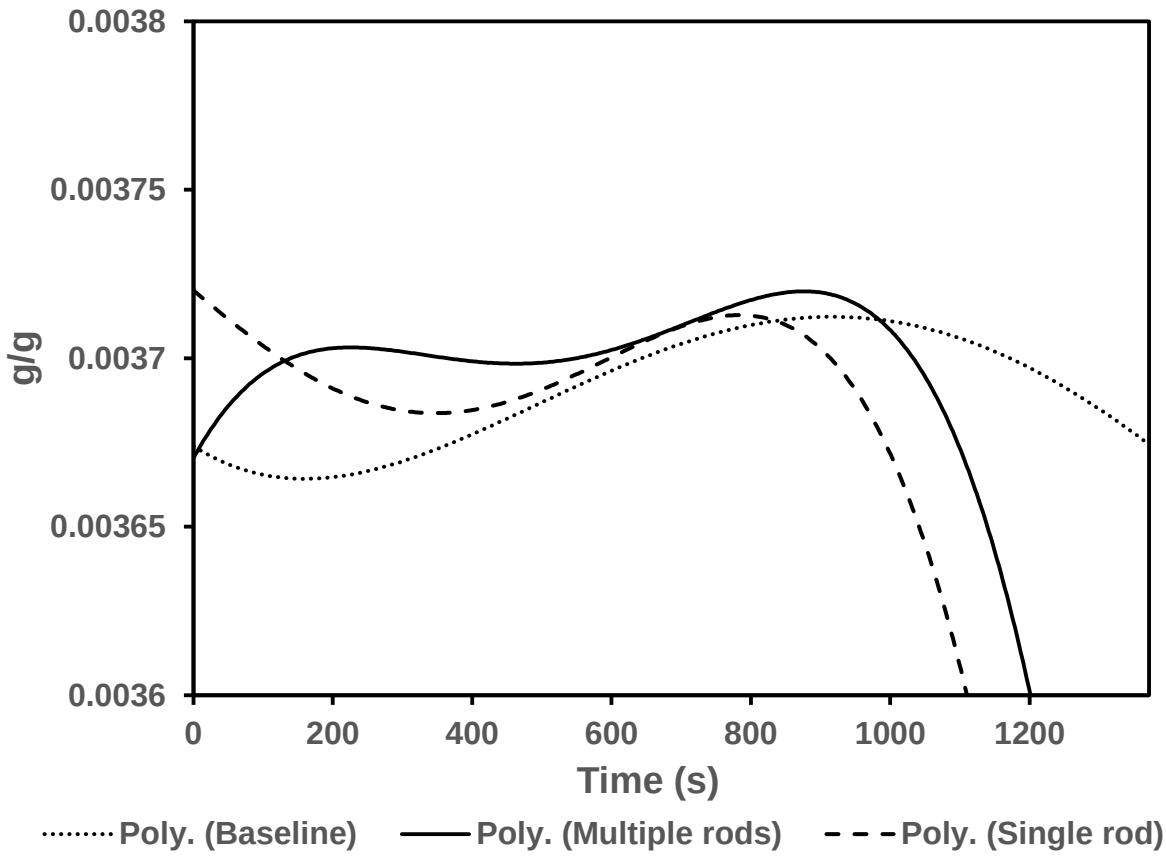

Figure 23: CO emission from 18% emulsion and 82% sand mixture burnt at 15 kW/m^2 heat flux

3.2 Discussions

In this section; ignition time, ignition temperature, mass loss and temperature distribution inside the mixture of 18% emulsion and 82% sand with 15 $\frac{kW}{m^2}$ heat flux is discussed for baseline and with immersed copper rods.

(Figure 24) shows the ignition time for three different cases (baseline, single immersed rod and immersed multiple rods of diameter 1cm). In the baseline, fuel is not ignited till the end of the experiment and is indicated by a hollow bar graph. With single immersed copper rod fuel is ignited at 540s. Multiple immersed rods (5 no's) of diameter 1cm, fuel

is ignited earlier compared with immersed single rod at 340s. An error is indicated on the bar graph to show the values of three repetitions.

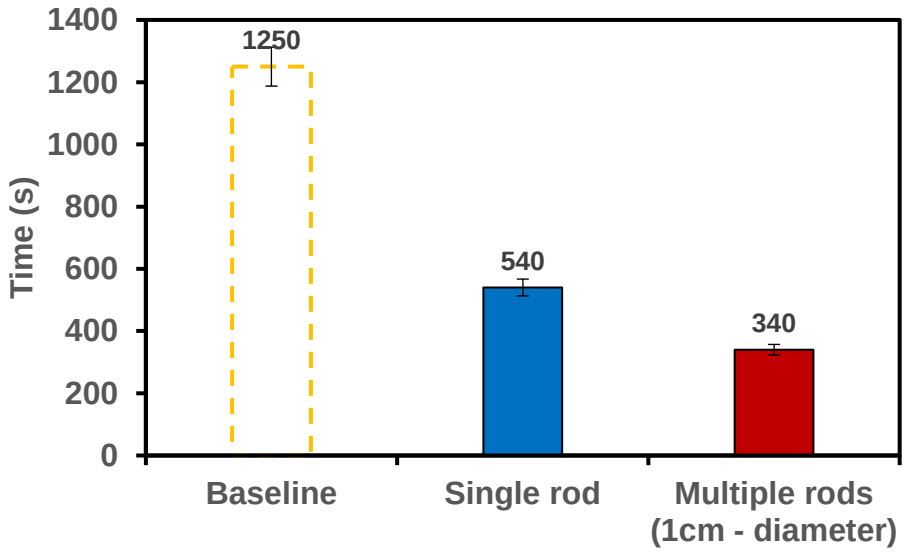

Figure 24: Comparison of ignition time

(Figure 25) shows the mass loss comparison for all the five different cases (baseline, single immersed rod, single rod of 10cm height, multiple immersed rods with 0.45cm and multiple immersed rods with 1cm diameter). The curves are fitted to the polynomial of the 4th degree. In Baseline tests, around 30g of the emulsion was burnt in the 1250s without any flame on the surface of the mixture. An error of 30 seconds is observed in three repetitions. The experiment is carried until 20% of the emulsion is left over in the mixture. With single immersed rod, a total mass of 31.3g ((87%) emulsion was burnt in 820s. Fuel is ignited at around 220℃ (210℃ - 220℃). An error of 15s to 30s is observed for fuel to burn 31.3g. With multiple rods of diameter 1cm, fuel ignited earlier and burnt with steady flames. Around 33.8g was burnt out of 34.2g emulsion (100%) fuel in 900s. The fuel did not ignite in the case of multiple rods with 0.45cm diameter and also for the case of rod immersed to a height of 10cm.

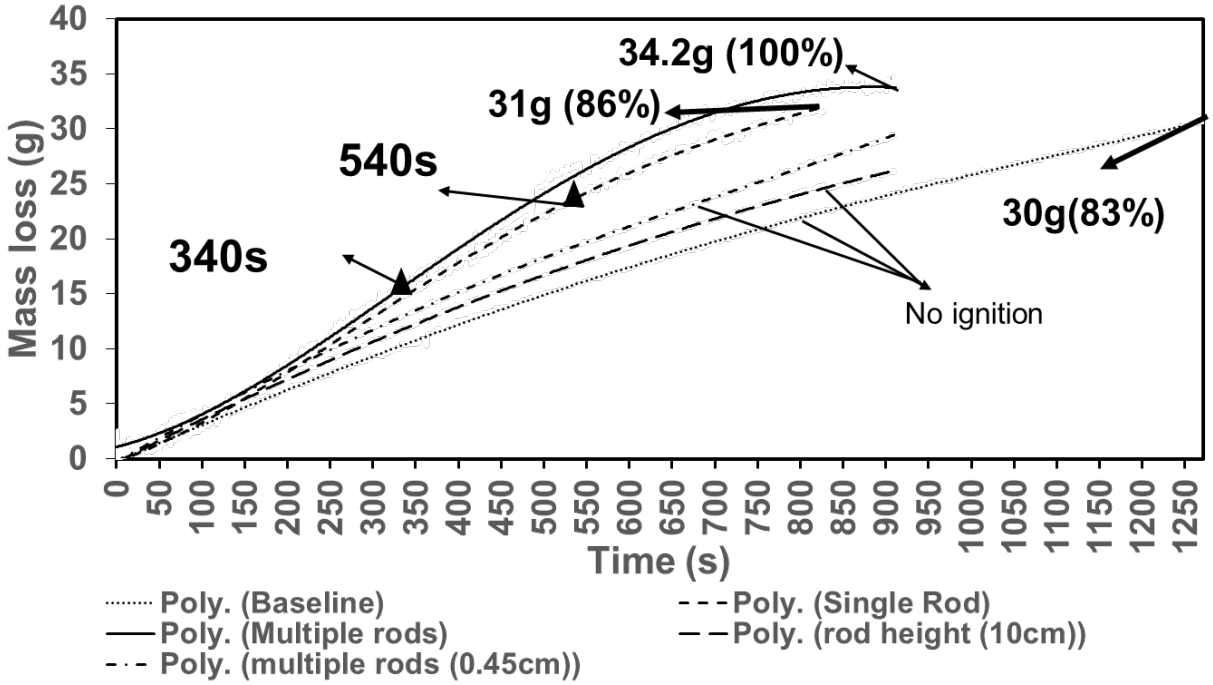

Figure 25: Comparison of mass loss

(Figures 26 and 27) show the flames at different time (100s, 200s, 600s, and 800s) instants for the cases with a single rod and multiple rods immersed in fuel (18% of emulsion & 82% sand) at $15\frac{kW}{m^2}$ heat flux. It can be seen that flames in Fig 24 are not stable. It is also seen that only the top layer of the fuel is burnt leaving behind some traces of emulsion in the fuel. Fuel after burning turns to a coal color and the unburnt fuel can be easily identified from it. Flames in Fig 25 are stable and intense hence results in complete combustion of the emulsion in fuel.

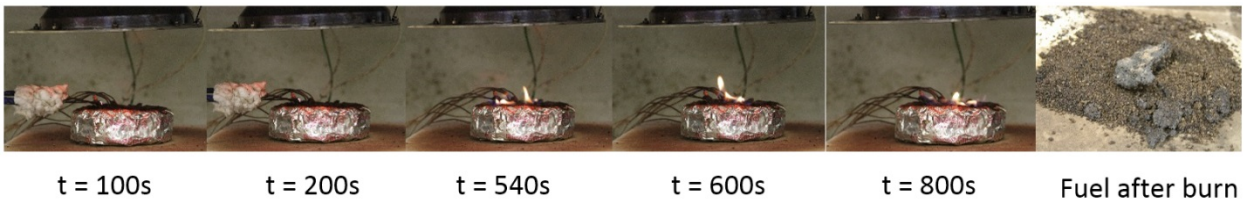

Figure 26: Fuel mixture burning at different time interval for single immersed copper rod test setup (heat flux- 15kW/m^2, case (a))

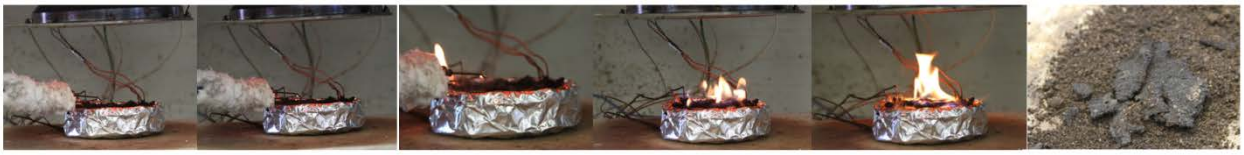

Figure 27: Fuel mixture burning at different time interval for multiple immersed copper rods test setup (heat flux- 15kW/m^2, case (a))

In these graphs, we can see that for baseline experiments the temperature of the fuel is always lesser compared with immersed copper rods. The temperature at the top surface is high because of flames burning the fuel. In baseline case, as there was no flames on the surface and only the radiative heat flux heating the fuel, the temperature is always lesser compared with immersed copper rods case.

In Fig. 28, at 100 s time during the test, all the temperature inside the fuel is in the same range. Only at the thermocouple placed at the top (0.2cm from the surface), temperature varies. At the center (1 cm from the surface) and bottom (1.8cm from the surface) of the fuel, there is some difference in temperature. In Fig. 29, at 200s time during the test, we can see that temperature increases at the top surface of the fuel for multiple immersed copper rods compared with the other two cases. Baseline case and the single rod immersed case are almost the same. Multiple copper rods heats the fuel faster compared with the other two cases.

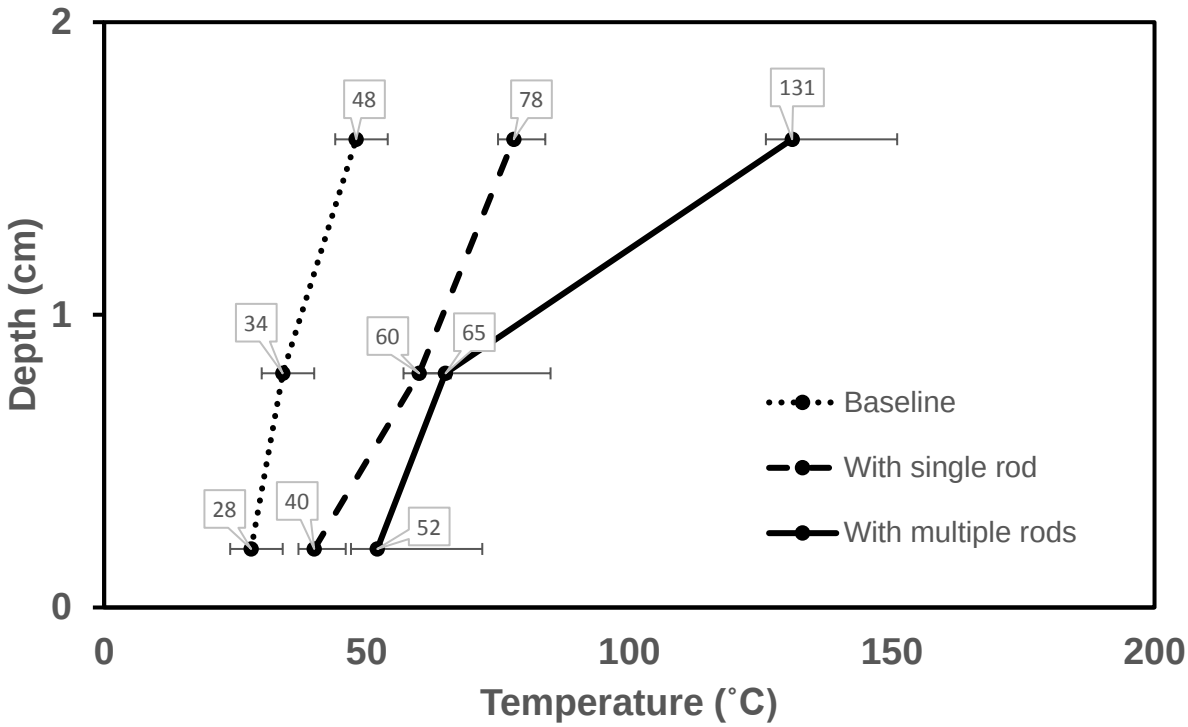

Figure 28: Temperature distribution in fuel at 100s

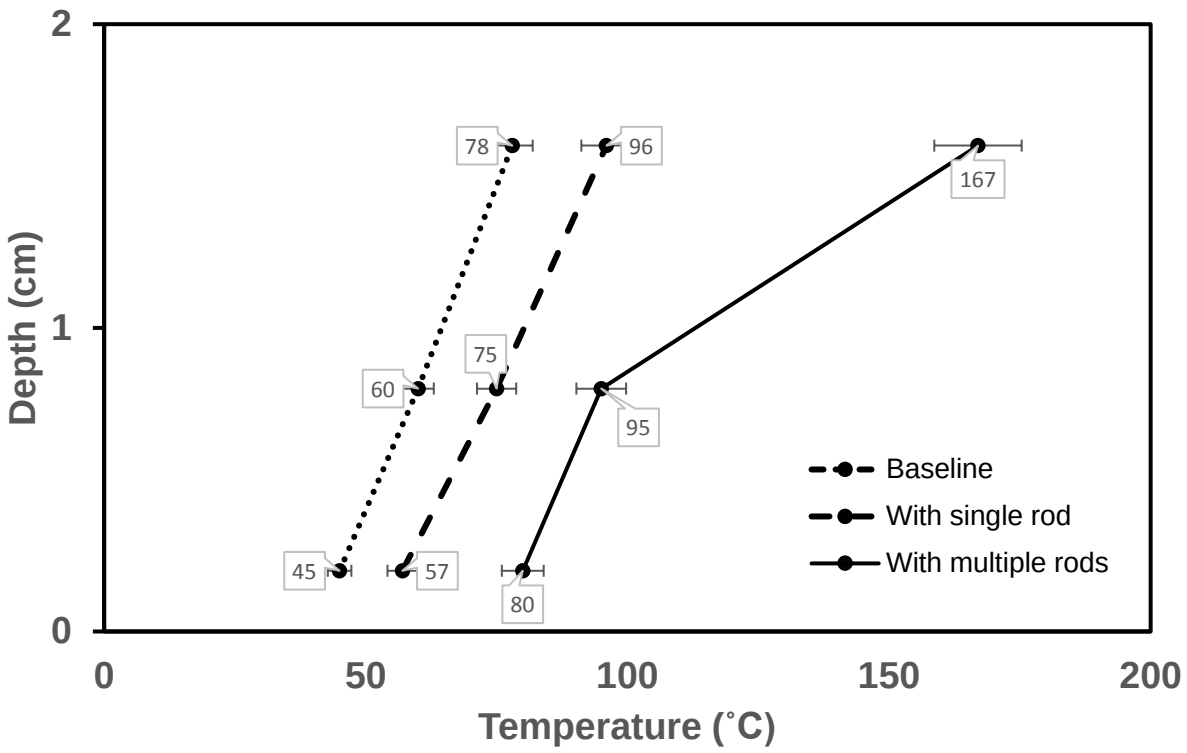

Figure 29: Temperature distribution inside the fuel at 200s

In Fig 30, at 600s during the test, fuel is ignited for both cases (single immersed rod and multiple immersed rod). The flame heats the fuel along with the radiative heat flux. Hence we can see the difference in the fuel temperature at both the top surface (0.2cm from the surface) as well as at the center (1cm from the surface) of the fuel. Whereas the temperature at the bottom (1.8cm from the surface) of the fuel mixture is still the same for baseline and single immersed rod.

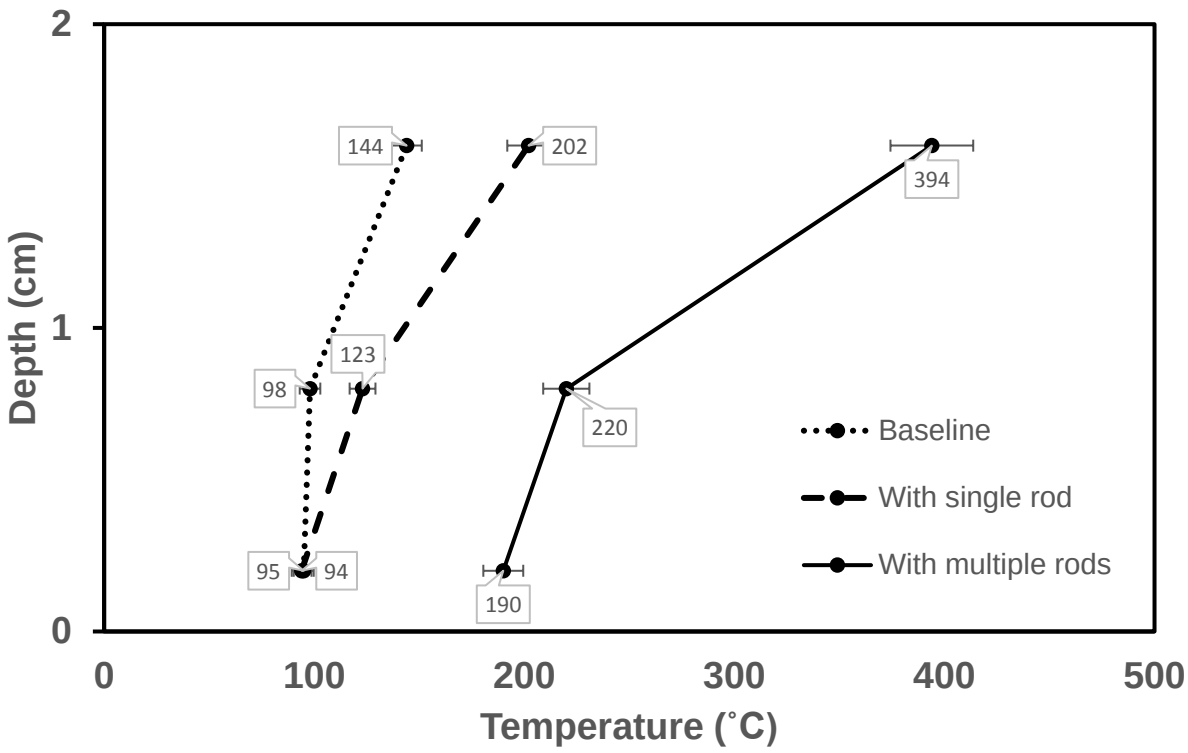

Figure 30: Temperature distribution inside the fuel at 600s

In Fig 31, at 800s during the test, flames are about to extinguish as the fuel is almost completely burned and little amount of emulsion remains. At this stage, fuel is completely heated till the bottom. Multiple copper rods immersed, heats the entire fuel mixture higher compared with the other two case. In the single immersed rod case as the flames are not intense and steady, the fuel is not much heated and traces of unburnt fuel (moisture content) can be seen in Fig 24. In the multiple immersed rods, flames are spread all over the surface of the fuel. During the burning process, the fuel shrinks as the emulsion is burned and fuel mixture solidifies.

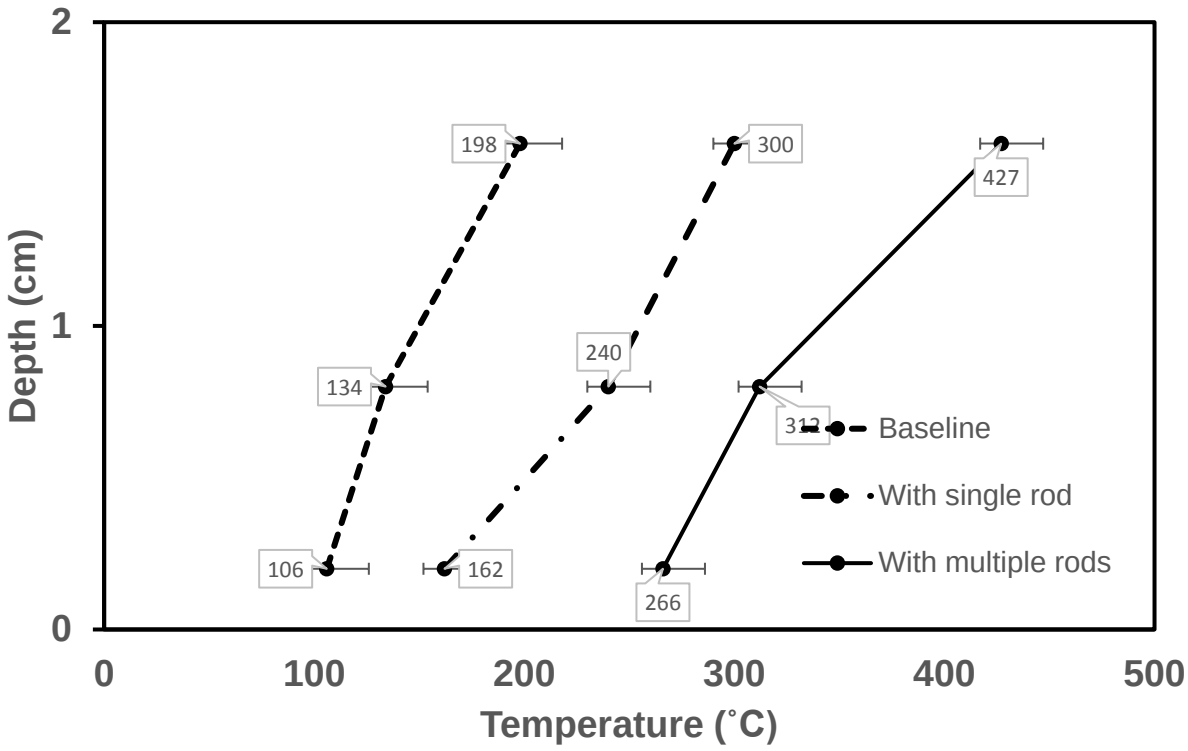

Figure 31: Temperature distribution inside the fuel at 800s

Chapter 4

4.1 Mathematical model

A mathematical model is an attempt to describe some part of the real world in mathematical terms [35]. Mathematical models can reveal the physics behind the experimental observations which can be used during the research and development of any product. Mathematical models are used to describe the behavior of results observed, predict the future behavior that is unseen or unmeasured [36]. Mathematical models are often used as it is faster than performing experiments. However, experiments are performed to validate the mathematical model. Once the mathematical model is validated, it can be used to study different cases without need of a new experiment.

The motivation behind this work is the need of such computational model that can explore the experimentally observed phenomena by means of a numeric model. To this end, a mathematical model based on conduction heat transfer is developed by using a finite volume method. The geometric details of the computational model and the thermophysical properties of the materials are discussed further.

Thermophysical properties of individual materials like copper, dry sand, salt water, and ANS crude oil is shown in table 13 [34, 37-43]. All the properties of the fuel mixture are calculated by the mass varied mixing method. Thermal properties of these materials vary with temperature [36, 44-46]. However, constant and steady state properties are assumed for this mathematical model.

The experimental setup is shown in the Figs 15-17 for baseline and immersed rod cases. The fuel surface is exposed to a uniform radiative heat flux from the cone heater. All the sides of the test pan are thermally insulated (Zero flux - Neumann boundary condition) for a thickness of 1cm. A cylindrical copper rod is immersed in the fuel mixture with its top surface exposed to radiative heat flux. The area of copper rod exposed to the heat flux is a collector (collects heat) and the surface of the fuel mixture

is the heater (heats the fuel around it). The heat transfer inside the copper rod is much faster than that of the sand and emulsion mixture, because of highly different thermal conductivities. Therefore deeply penetrated heat inside the copper rod can lead heat conduction from the rod surface to sand-emulsion mixture at the region close to pan bottom.

Two heat transfer mechanisms are available for experimental setups used in the experiments; (i) smouldering combustion till the flames appear on the fuel surface, (ii) combustion by flames. In smouldering combustion process, in which the fuel is heated only by a uniform radiative heat flux, the fuel is either smouldered or evaporated. During flaming combustion, the fuel is heated by the visible flame and the uniform heat flux from the cone heater. It is also observed that conduction heat transfer is dominant between the fuel and copper rods during the experiment. Heat from the flame and cone heater results in a larger burning rate compared with smouldering combustion process in which only the heat transfer from the cone heater is available.

Table 13: Thermal properties of materials used in experiments [34, 37-43]

	Thermal conductivity ($\frac{W}{m\,K}$)	**Density ($\frac{kg}{m^3}$)**	**Specific heat capacity ($\frac{J}{k_g K}$)**
Dry sand	0.16	1920	830
ANS crude oil	0.132	868	2300
salt water	0.6	1025	3850
Copper	385	8950	385
Water in oil emulsion[7]	0.4128	962.44	3230
Fuel (lower emulsion content)[8]	0.2055	1747.6	1262
Fuel (higher emulsion content)[9]	0.22	1690.2	1406

[7] Crude oil - 40% and Salt water – 60% by mass.
[8] 18% emulsion and 82% sand
[9] 24% emulsion and 76% sand

4.1.1 Problem description

In the present study, experimentally observed temperature distribution inside the fuel at a different time is analyzed by a numerical method [47]. Influence of a number of the immersed copper rods is predicted for different heat fluxes. The temperature distribution inside the sand-emulsion mixture is calculated during the burning process. The detail of the numerical model is given in the following sections.

Heat transfer mechanism is shown in the following Fig 32 & 33 for baseline and single immersed rod ($\emptyset - 1cm$). In the present study, the amount of the sand used in the experiments is much higher than that of emulsion. Therefore, the convection heat transfer inside the sand-emulsion mixture is considered to be negligible. The heat transfer inside the experimental setup is assumed to be only by conduction. In order to ensure the energy conservation, the 2-D energy equation is discretized by finite volume method with appropriate initial and boundary conditions.

4.1.2 Finite Volume method for two-dimensional unsteady conduction

(Figure 32) shows a schematic representation of heat transfer for the baseline test setup. The test setup is discretized in x and y-direction by a number of grid points. The area under each grid point is known as control volume (CV) and calculated by the product of $\Delta \mathrm{x}\, \Delta \mathrm{y}$. Grid point P is considered to be the center, E, and W grid points are its neighbors in x- direction. Grid points N and S are neighbors in the y-direction. The distance between each grid point is Δx in x-direction and Δy in y-direction. Grid point P is located at the position (i, j), W at (i-1, j), E at (i+1, j), N at (i, j+1) and S is located at (i, j-1). The control volume boundaries are indicated as w, e, n and s in respective directions [47].

Transport equation (Eq. 1) for the transient heat transfer inside the sand-emulsion mixture is solved by finite volume method [48]. Discretized control volume is shown in the following figure.

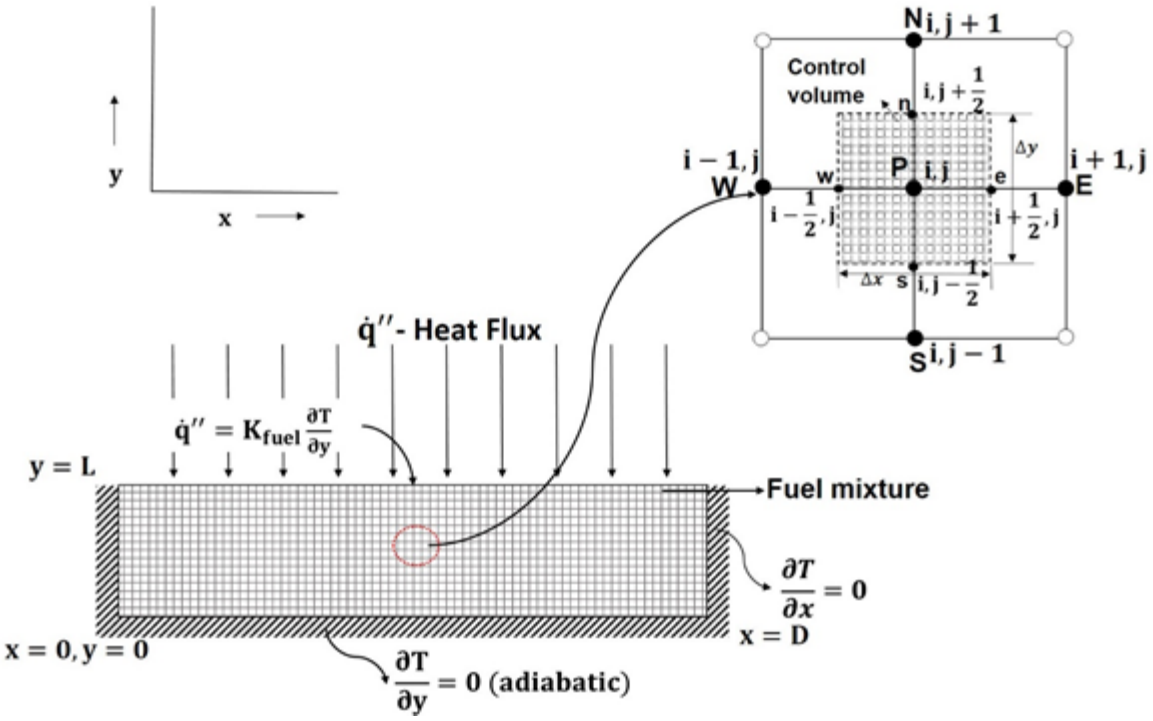

Figure 32: Schematic representation of the porous fuel geometry and the extracted computational cell for control volume approach (baseline)

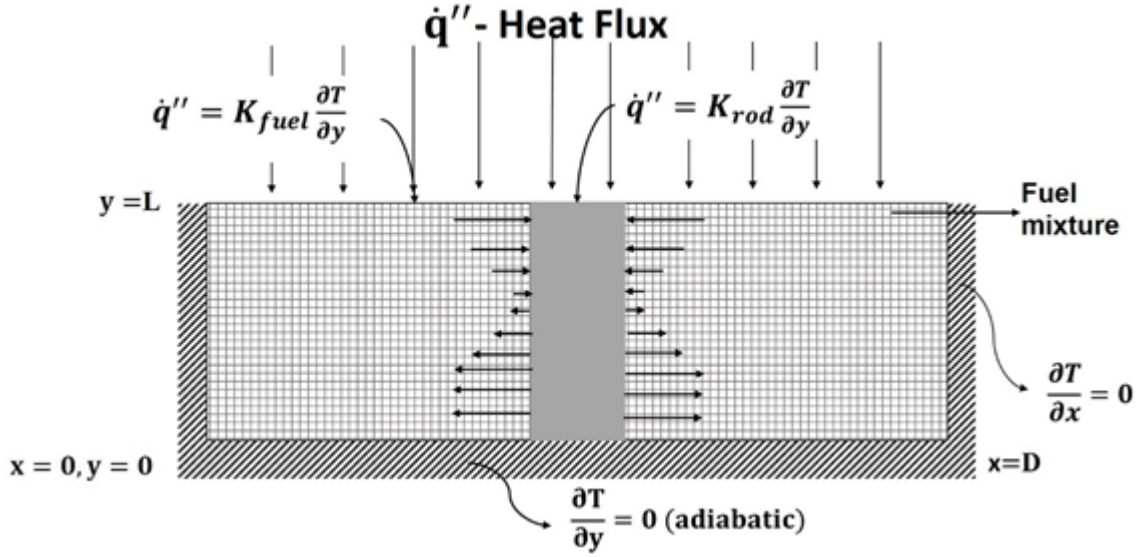

Figure 33: Schematic representation of the porous fuel geometry and the extracted computational cell for control volume approach (immersed rod)

$$\rho c_p \frac{\partial T}{\partial t} = \frac{\partial}{\partial x} k \frac{\partial T}{\partial x} + \frac{\partial}{\partial y} k \frac{\partial T}{\partial y} + S, \quad (1)$$

with no internal heat source $(S = 0)$

The above equation reduces to

$$\rho c_p \frac{\partial T}{\partial t} = \frac{\partial}{\partial x} k \frac{\partial T}{\partial x} + \frac{\partial}{\partial y} k \frac{\partial T}{\partial y}. \quad (2)$$

The discretization equation is now derived by integrating (eq 2) over the control volume. Order of the integration is also chosen according to the nature of the term. The temperature at the grid point is assumed to prevail throughout the control volume. Hence we get

At LHS

$$\rho c_p \int_{x_i}^{x_{i+1}} \int_{y_j}^{y_{j+1}} \frac{\partial T}{\partial t} \, dx \, dy = \rho c_p \frac{\Delta x \, \Delta y}{\Delta t} \left(T_p - T_p{}^o\right), \quad (3)$$

RHS:

$$\int_{x_i}^{x_{i+1}} \int_{y_j}^{y_{j+1}} \frac{\partial}{\partial x} K \frac{\partial T}{\partial x} \, \partial x \, \partial y + \int_{x_i}^{x_{i+1}} \int_{y_j}^{y_{j+1}} \frac{\partial}{\partial y} K \frac{\partial T}{\partial y} \, \partial x \, \partial y \ , \quad (4)$$

$$\int_{y_j}^{y_{j+1}} \left(K \frac{\partial T}{\partial x_e}\right) - \left(K \frac{\partial T}{\partial x_w}\right) \partial y + \int_{x_i}^{x_{i+1}} \left(K \frac{\partial T}{\partial y_n}\right) - \left(K \frac{\partial T}{\partial y_s}\right) \partial x \ ,$$

$$\int_{y_j}^{y_{j+1}} K_e \frac{(T_E - T_P)}{\delta x_e} - K_w \frac{(T_P - T_W)}{\delta x_w} \partial y + \int_{x_i}^{x_{i+1}} K_n \frac{(T_N - T_P)}{\delta y_n} - K_s \frac{(T_P - T_S)}{\delta y_s} \partial x,$$

$$K_e \frac{(T_E - T_P)}{\delta x_e} \Delta y - K_w \frac{(T_P - T_W)}{\delta x_w} \Delta y + K_e \frac{(T_N - T_P)}{\delta y_e} \Delta x - K_w \frac{(T_P - T_S)}{\delta y_w} \Delta x. \quad (5)$$

By equating Eq 3 & Eq 5, we get discretization equation in the form of:

$$a_p T_p = a_E T_E + a_W T_W + a_N T_N + a_S T_S + a^0{}_p T^0{}_p. \quad (6)$$

where:

$$a_E = \frac{K_e}{\delta x_e}\Delta y,$$

$$a_W = \frac{K_w}{\delta x_w}\Delta y,$$

$$a_N = \frac{K_n}{\delta y_n}\Delta x,$$

$$a_S = \frac{K_s}{\delta y_s}\Delta x,$$

$$a^0{}_p = \frac{\rho c\, \Delta x\, \Delta y}{\Delta t}.$$

$$a_P = a_E + a_W + a_N + a_S + a^0{}_p$$

This equation gives the discretization for internal grid points. A fully implicit Euler's method is used for the time integration and a direct matrix solver available in MATLAB® library is used for the coefficient matrix of the 2D energy equation.

The boundary conditions are:

$$x = 0, \qquad \frac{\partial T}{\partial x} = 0,$$

$$y = 0, \qquad \frac{\partial T}{\partial y} = 0,$$

$$y = L, \qquad \dot{q}'' = K_{fuel}\frac{\partial T}{\partial y},$$

$$x = D, \qquad \frac{\partial T}{\partial x} = 0.$$

4.2 Model Assumptions

In present study, the following assumptions are considered

1. Reflection and re-radiation from the surface is ignored $(q'_{r,f-sur})$ and $(q'_{or,f-sur})$.
2. Constant properties are used in the model as shown in Table 13. The thermal conductivity of crude oil, water and sand is a function of temperature and composition. These effects are ignored and a constant thermal conductivity calculated at 20 ºC is assumed.
3. Zero-flux Neumann boundary conditions are assumed at the bottom and surface of the test pan as shown in Fig 30 and 31. Even though the surface has some heat losses the effect is ignored.
4. Phase change for emulsion mixture at higher temperature is neglected.

4.3 Model results

The numerical model used in the present study is coded in MATLAB®. (Figures 34 – 37) show a representation of temperature distribution inside the fuel mixture at different heat fluxes. The comparison is made between three different experimental test setups. In the baseline test setup, the temperature distribution inside the sand-emulsion mixture is uniform in horizontal direction. In the single and multiple immersed rod test setups, increase in the temperature region around the copper rod is visually seen. Temperature is, even more, higher and widely distributed around the multiple copper rods.

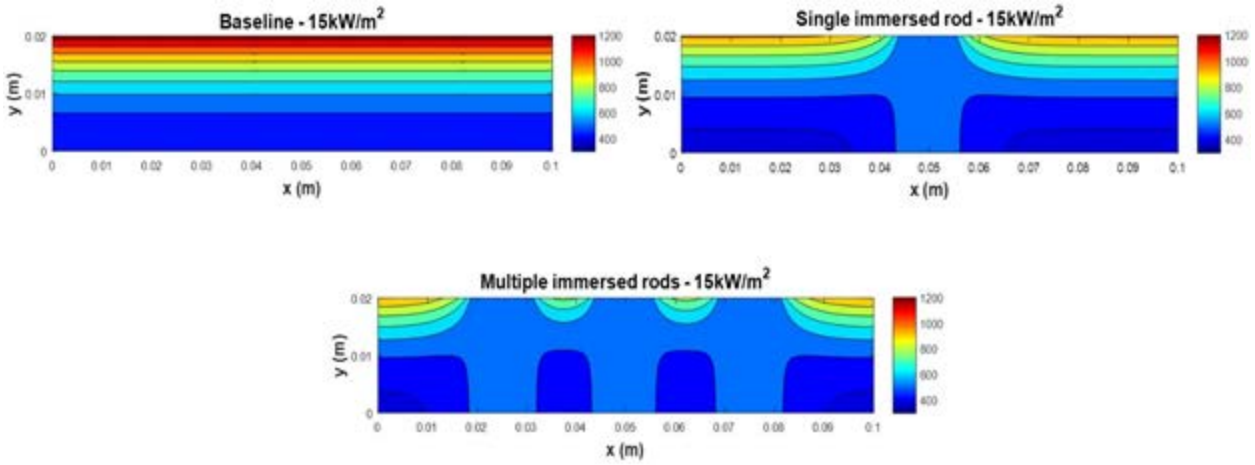

Figure 34: Schematic representation of temperature distribution inside fuel bed for baseline and immersed rods case for 18% emulsion and 82% sand at 15kW/m^2

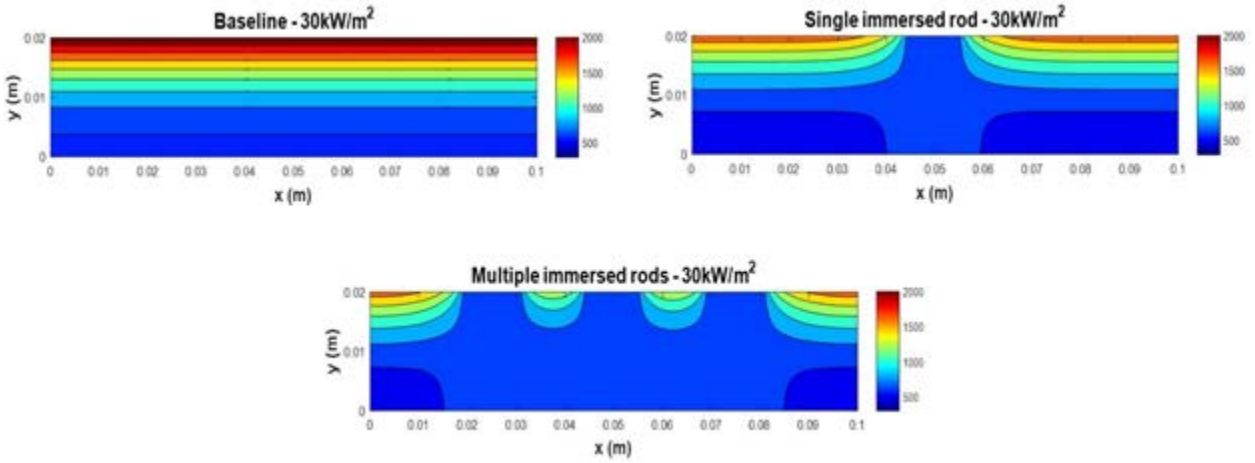

Figure 35: Schematic representation of temperature distribution inside fuel bed for baseline and immersed rods case for 18% emulsion and 82% sand at 30kW/m^2

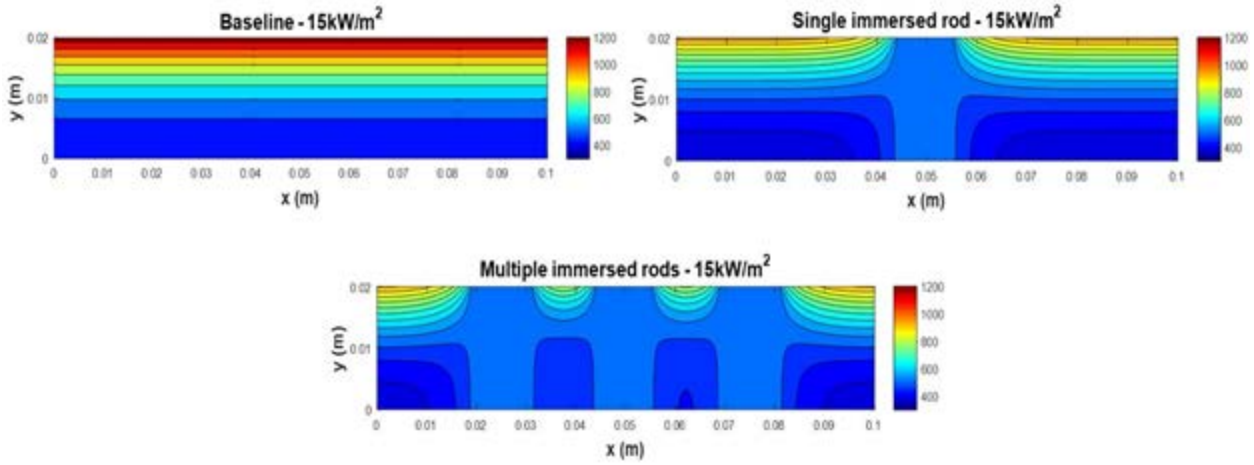

Figure 36: Schematic representation of temperature distribution inside fuel bed for baseline and immersed rods case for 24% emulsion and 76% sand at 15kW/m^2

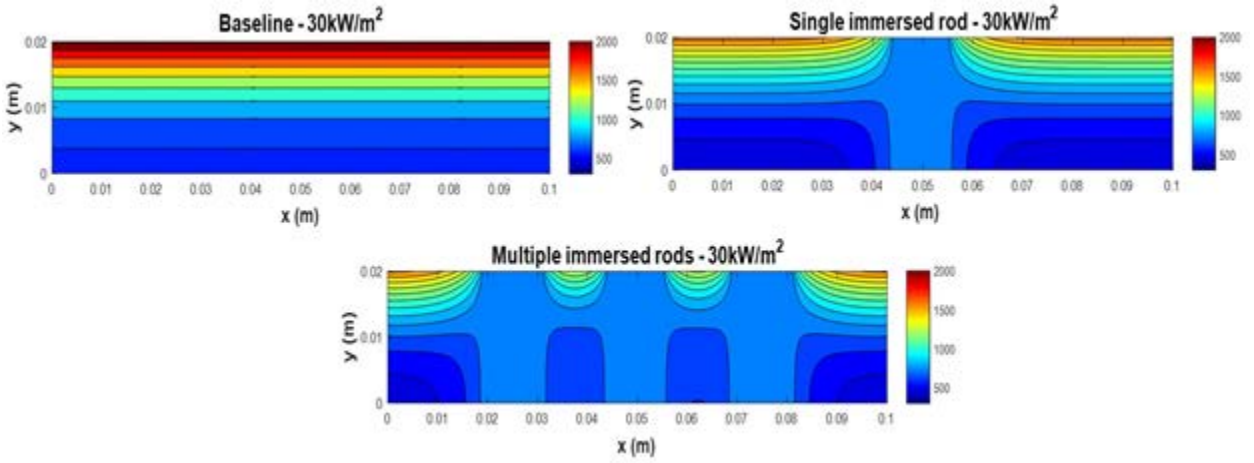

Figure 37: Schematic representation of temperature distribution inside fuel bed for baseline and immersed rods case for 24% emulsion and 76% sand at 30kW/m^2

(Figure 38) shows the change in temperature with respect to time at different locations inside the sand-emulsion mixture. The locations at which the temperature is measured is measured is shown in Fig 16, 17 & 18 for baseline, single immersed rod, and multiple immersed rod cases. From the Figures, it can be seen that, in the baseline case, the temperature at the bottom of fuel mixture takes around 400s to start heating. In the

single immersed rod case, the temperature at the bottom of fuel mixture starts to increase earlier around 300s. For the multiple immersed rods case, temperature at the bottom of the fuel starts to increase around 100s, this clearly shows that copper rods heat the fuel mixture in a shorter period of time compared with the baseline case.

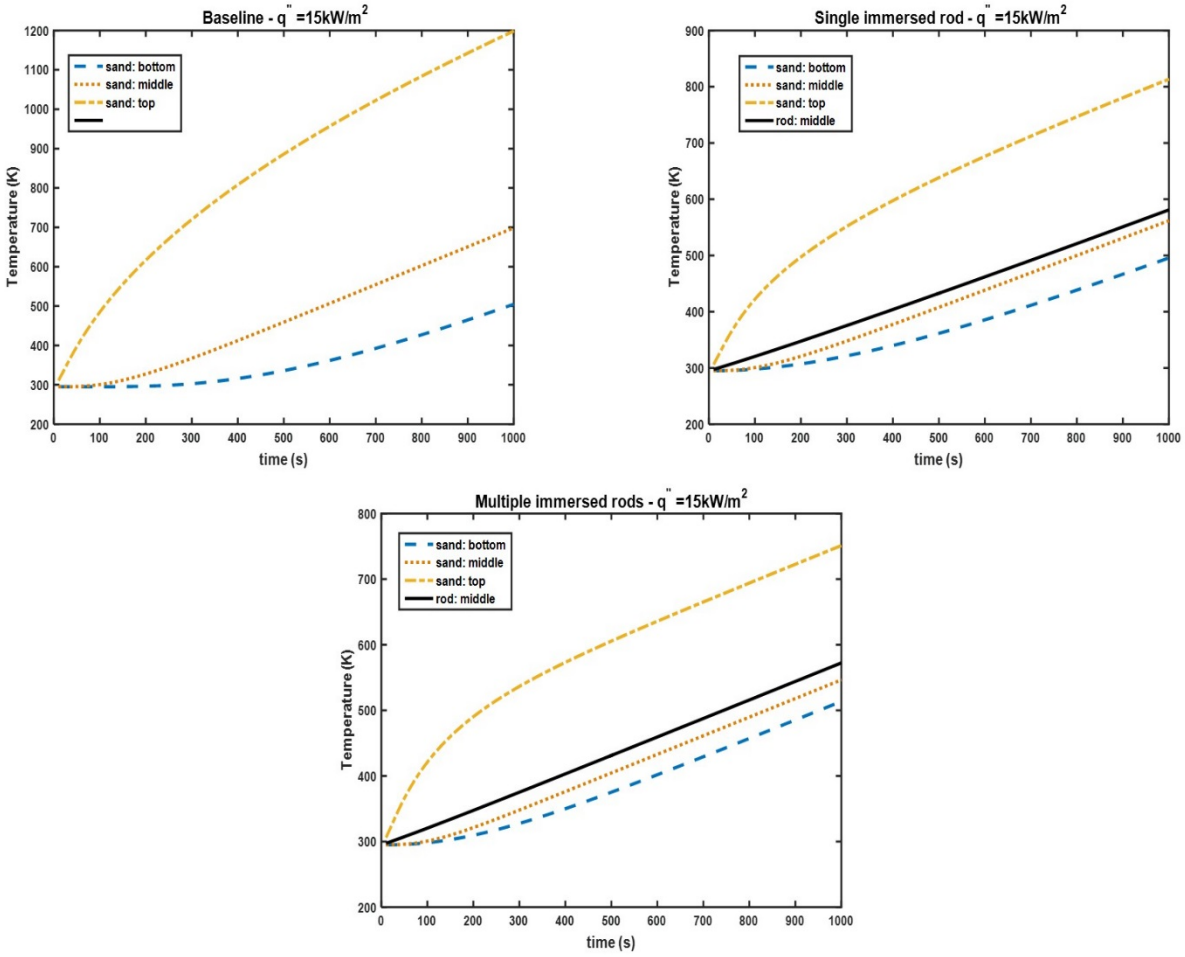

Figure 38: Schematic representation of temperature plots at different locations inside the fuel mixture for 18% emulsion with 82% sand

Chapter 5

Conclusions & Future work

To explore the effect of immersed conductive objects on burning behavior of contaminated sand, bench scale experiments ($\emptyset - 10cm$) were performed of varying emulsion content (18% and 24%) in the fuel mixture. Various heat fluxes (15, 20, 25 and 30$\frac{kW}{m^2}$) and different rod configurations (single rod, multiple rods and cases with various rod heights and diameters) were studied. The impact on ignition time, mass loss and temperature profiles were investigated. The mass burning rate is primarily enhanced by copper rods and limited by the water content inside the fuel mixture. Immersed copper rods show a significant improvement in ignition time (fuel ignites in shorter time), and mass burning rate. However, higher the emulsion content in the fuel takes more time for the fuel to ignite as the water content in the fuel mixture also increases. A complete (100%) combustion was seen in immersed rod cases for both fuel mixtures (lower and higher emulsion content in fuel). Temperature inside the fuel mixture is increased with the influence of immersed copper rods. However, a significant increase in temperature inside the fuel mixture cannot be seen at higher heat flux (25 and 30kW/m^2) as the heat flux itself is dominant. The test sample was too small to observe any influence. The model is simulated to show the influence of copper rods inside the fuel mixture. Model shows increase in fuel temperature around the surface of copper rod inside the fuel mixture. The predictions of the model are in a good agreement with the experimental data. However, the model could be improved by incorporating other physical phenomena i.e. phase change of the fuel mixture, thermophysical properties changing w r t time and temperature, burning rate and change in geometry and dimensions of the copper rods for achieving higher efficiency. Experiments have to be conducted without any external heat flux and observe the behavior of copper rods in combustion i.e. to perform tests that are more similar to a realistic oil spill incident

References

1. Evans, D.D., et al., *In situ burning of oil spills.* Journal of Research-National Institute of Standards and Technology, 2001. **106**(1): p. 231-278.
2. Allen, A.A. *Controlled burning of crude oil on water following the grounding of the Exxon Valdez*. in *International Oil Spill Conference*. 1991. American Petroleum Institute.
3. Ali S Rangwala, Kemal S Arsava., Mahnken G, Xiaochuan, *A Novel Experimental Approach to Enhance Burning Of Oil-Water Emulsions by Immersed Objects*. 2015, Department of Fire Protection Engineering, Worcester Polytechnic Institute: Worcester.
4. Holba, C., *Exxon Valdez oil spill: FAQs, links, and unique resources at ARLIS.* Anchorage: Alaska Resources Library & Information Services, 2014.
5. Walther III, H.R., *Clean Up Techniques Used for Coastal Oil Spills: an Analysis of Spills Occurring in Santa Barbara, California, Prince William Sound, Alaska, The Sea of Japan, and the Gulf Coast.* 2014.
6. Clarke, K.C. and J.J. Hemphill, *The Santa Barbara oil spill: A retrospective.* Yearbook of the Association of Pacific Coast Geographers, 2002. **64**(1): p. 157-162.
7. Cooper, L., *Oil spill reported on coast near refugio state beach*. 2015.
8. Kacik, A. *3 months after oil spill, Santa Barbara region recovering*. 2015 [cited 2016 7/16]; Available from: http://www.pacbiztimes.com/2015/08/14/3-months-after-oil-spill-santa-barbara-region-recovering/.
9. Campbell, R. and K. Clifford, *Gulf spill is the largest of its kind, scientists say.* The New York Times, 2010. **7**: p. 2010.
10. Norse, E.A. and J. Amos, *Impacts, perception, and policy implications of the Deepwater Horizon oil and gas disaster.* Environmental Law Institute, Washington, DC, 2010. **40**: p. 11058.
11. Kerr, R.A., *A lot of oil on the loose, not so much to be found.* Science, 2010. **329**(5993): p. 734-735.

12. MacPHERSON, J. *ND farmer finds oil spill while harvesting wheat*. [cited 2013 11]; Available from: http://www.breitbart.com/news/da9c0afg0/.
13. Clark, T. and R.D. Martin Jr. *In Situ Burning: After-Action Review 1 (Successful Burn 48 Hours After Discharge)*. in *International Oil Spill Conference*. 1999. American Petroleum Institute.
14. J. MICHEL, D.S., S.R. WARREN JR., AND A.H. WALKER, *IN-SITU BURNING*, in *A DECISION-MAKER'S GUIDE TO IN-SITU BURNING*. 2005, Regulatory and Scientific Affairs Department: Washington.
15. Rutherford, J.M.a.N., *Oil Spills in Marshes*. 2013, Research Planning, Inc.
16. Gonzalez, M.F. and G.A. Lugo. *Texas marsh burn: Removing oil from a salt marsh using in situ burning*. in *International Oil Spill Conference*. 1995. American Petroleum Institute.
17. team, h.s.c. *The Largest Oil Spills in History*. 2010; Available from: http://chartsbin.com/view/mgz.
18. Guard, U.S.C. *How Do Oil Spills Get Cleaned up on Shore?* 2015; Available from: http://response.restoration.noaa.gov/about/media/how-do-oil-spills-get-cleaned-shore.html.
19. bianoti. *Oil Spill Skimmers*. 2016; Available from: http://www.bianoti.com/oil-spill-skimmers.html.
20. *Oil spills in the water ways*. 2016; Available from: http://scienceproject-ceyerra.weebly.com/how-has-chemistryscience-contributed-to-this-issue.html.
21. ANDREI, M. *BioRemediation in Manila, Philippines*. 2013 [cited 2016 7/17]; Available from: http://www.zmescience.com/ecology/bioremediation-in-manila-philippines/.
22. Ottery, C. *In situ burning* 2015 [cited 2015 15]; Available from: http://energydesk.greenpeace.org/2015/04/15/factcheck-how-to-clean-up-an-arctic-oil-spill-in-four-steps-and-why-it-is-unlikely-to-work/.
23. Meikle, K. and H. Ewing. *Oil spill incinerator development: and update*. in *Proceedings of the Third Arctic Marine Oilspill Program Technical Seminar. Environmental Protection Service, Ottawa*. 1980.

24. Pertile, L. *In-situ combustion of stranded oil on remote shorelines*. in *Proceedings of the Ninth*. 1986.
25. Nelson P. Bryner, W.D., Walton, William H. Twilley, and Gary Roadarmel. *In-situ Burning in the Marshland Environment- Soil Temperatures Resulting from crude oil and Diesel Fuel Burns*. in *Proceedings of the Twenty-fourth Arctic and Marine Oilspill Program (AMOP) Technical Seminar*. 2001. Edmonton(Alberta) Canada: Environment Canada.
26. Fatemi, S.M., et al. *Application of Toe-to-Heel Air Injection (THAI) Process in Fractured Carbonate Systems: 3D Simulation of the Effect of Fractures Geometrical Properties, Reservoir and Operational Parameters*. in *SPE EUROPEC/EAGE Annual Conference and Exhibition*. 2011. Society of Petroleum Engineers.
27. Shojaiepour, M., et al., *Experimental and Simulation Study of In-situ Combustion Process in Carbonate Fractured Porous Media.* Journal of the Japan Petroleum Institute, 2014. **57**(5): p. 208-215.
28. Xia, T.X., Greaves, M., Werfilli, S.M., Rathbone R. *THAI process- Effect of the oil layer thickness on heavy oil recovery*. in *Canadian International Petroleum Conference*. 2002. Calgary, Alberta, Canada.
29. Pironi, P., *Smouldering Combustion of Organic Liquids in Porous Media for Remediating NAPL-contaminated Soils.* 2010.
30. Ohlemiller, T.J., *Modeling of smoldering combustion propagation.* Progress in Energy and Combustion Science, 1985. **11**(4): p. 277-310.
31. P, P., *Smouldering Combustion of Organic Liquids in Porous media for Remediating NAPL-contaminated Soils*. 2009: Edinburgh.
32. Lindholm, J., A. Brink, and M. Hupa, *Cone Calorimeter—A Tool for Measuring Heat Release Rate.* Åbo Akademi Process Chemistry Centre, Finland, 2009.
33. Babrauskas, V., *Heat release rates*, in *SFPE handbook of fire protection engineering*. 2016, Springer. p. 799-904.
34. Torero, J.L., et al., *Determination of the burning characteristics of a slick of oil on water.* Spill Science & Technology Bulletin, 2003. **8**(4): p. 379-390.
35. Meyer, W.J., *Concepts of mathematical modeling*. 2012: Courier Corporation.

36. Carrejo, D.J. and J. Marshall, *What is mathematical modelling? Exploring prospective teachers' use of experiments to connect mathematics to the study of motion.* Mathematics Education Research Journal, 2007. **19**(1): p. 45-76.
37. Hamdhan, I.N. and B.G. Clarke. *Determination of thermal conductivity of coarse and fine sand soils*. in *Proceedings of World Geothermal Congress*. 2010.
38. Quick, R., C. Child, and B. Lanphear, *Thermal Conductivity of Copper.* Physical Review (Series I), 1895. **2**(6): p. 412.
39. Caldwell, D.R. *Thermal conductivity of sea water*. in *Deep Sea Research and Oceanographic Abstracts*. 1974. Elsevier.
40. Millero, F.J., A. Gonzalez, and G.K. Ward, *DENSITY OF SEAWATER SOLUTIONS AT ONE ATMOSPHERE AS A FUNCTION OF TEMPERATURE AND SALINITY.* Journal of Marine Research, 1976. **34**(1): p. 61-93.
41. Martin, D.L., *THE SPECIFIC HEAT OF COPPER FROM 20° TO 300 deg; K.* Canadian Journal of Physics, 1960. **38**(1): p. 17-24.
42. Millero, F.J., G. Perron, and J. Desnoyers, *Heat capacity of seawater solutions from 5° to 35° C and 0.5 to 22‰ chlorinity.* Journal of geophysical research, 1973. **78**(21): p. 4499-4507.
43. Farouki, O.T., *Thermal properties of soils.* 1986.
44. Ozbek, H. and S. Phillips, *Thermal conductivity of aqueous NaCl solutions from 20 {sup 0} C to 330 {sup 0} C*. 1979, California Univ., Berkeley (USA). Lawrence Berkeley Lab.
45. Sharqawy, M.H., J.H. Lienhard, and S.M. Zubair, *Thermophysical properties of seawater: a review of existing correlations and data.* Desalination and Water Treatment, 2010. **16**(1-3): p. 354-380.
46. Powell, R., C.Y. Ho, and P.E. Liley, *Thermal conductivity of selected materials*. 1966, DTIC Document.
47. Patankar, S., *Numerical heat transfer and fluid flow*. 1980: CRC press.
48. Eymard, R., T. Gallouët, and R. Herbin, *Finite volume methods.* Handbook of numerical analysis, 2000. **7**: p. 713-1018.

APPENDIX A

Ignition time for the three repetitions performed for all the experimental cases.

Table A 1: ignition time - baseline case for two different fuel mixtures

Heat flux ($\frac{kW}{m^2}$)	Baseline (s) – lower emulsion content			Baseline (s) - higher emulsion content		
	Test 1	**Test 2**	**Test 3**	**Test 1**	**Test 2**	**Test 3**
15kW/m²	No flame	No flame	No flame	484	472	455
20kW/m²	242	246	236	390	381	378
25kW/m²	158	150	145	325	300	328
30kW/m²	130	138	138	296	287	282

Table A 2: ignition time - immersed single rod case for two different fuel mixtures

Heat flux ($\frac{kW}{m^2}$)	Single immersed rod (s) – lower emulsion content			Single immersed rod (s) - higher emulsion content		
	Test 1	**Test 2**	**Test 3**	**Test 1**	**Test 2**	**Test 3**
15kW/m²	552	536	532	442	415	440
20kW/m²	183	180	180	326	320	320
25kW/m²	108	108	114	242	248	239
30kW/m²	85	85	85	180	180	178

Table A 3: ignition time – multiple immersed rods case for two different fuel mixtures

Heat flux ($\frac{kW}{m^2}$)	Multiple immersed rods (s) – lower emulsion content			Multiple immersed rods (s) - higher emulsion content		
	Test 1	**Test 2**	**Test 3**	**Test 1**	**Test 2**	**Test 3**
15kW/m²	344	340	338	411	441	426
20kW/m²	170	178	178	319	324	311
25kW/m²	108	104	108	243	228	225
30kW/m²	85	85	85	172	177	184

Mass loss of the fuel

i. Baseline case: lower emulsion content and higher emulsion content

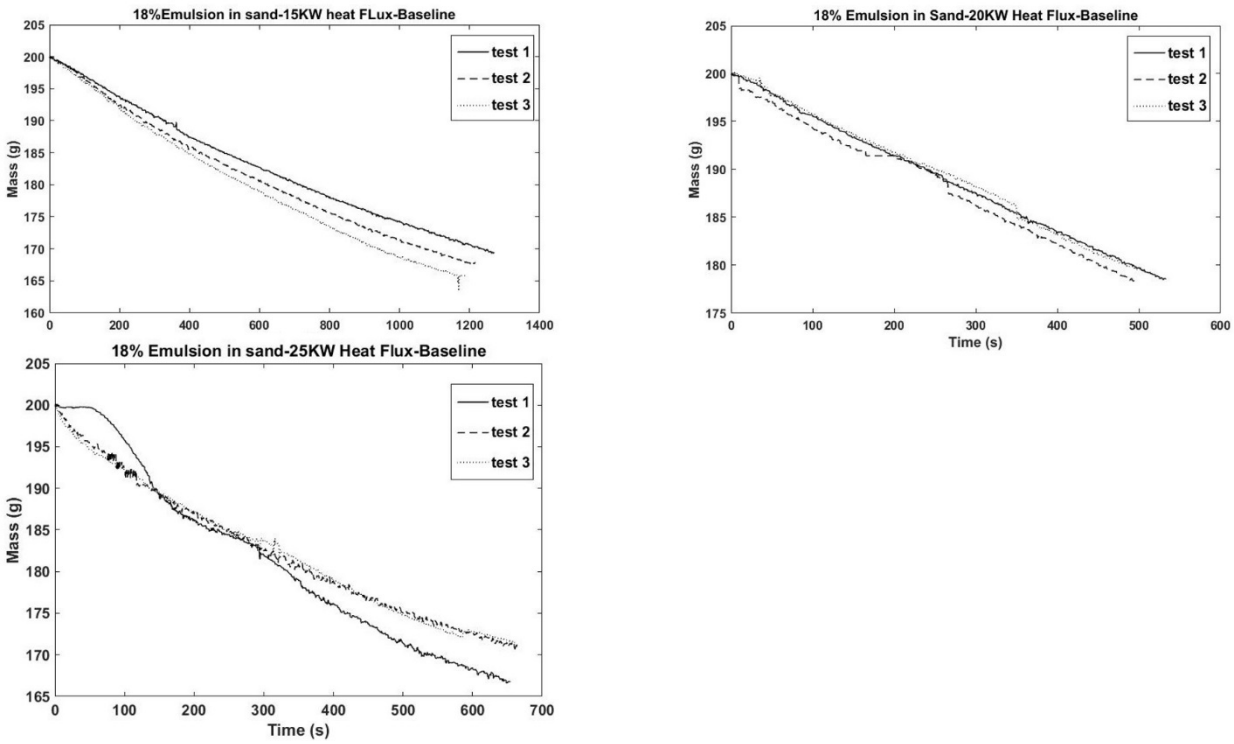

Figure A 1: Mass loss - baseline case (lower emulsion content)

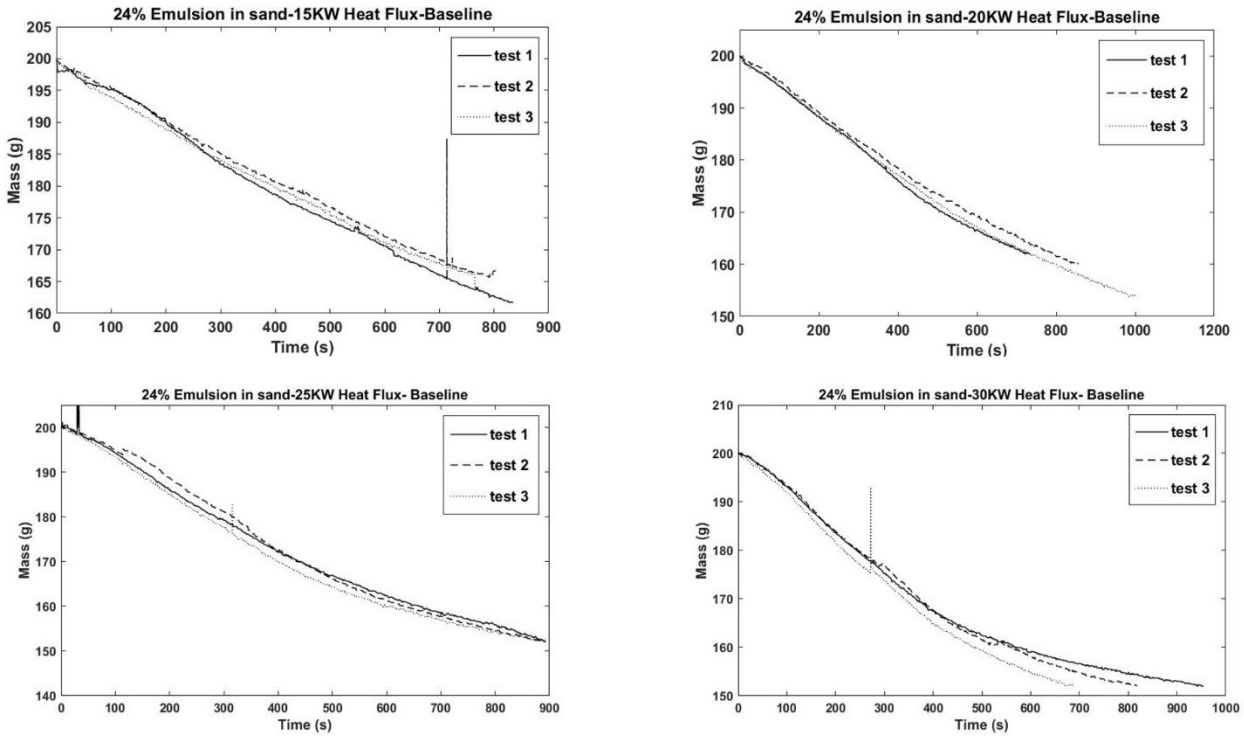

Figure A 2: Mass loss - baseline case (Higher emulsion content)

ii. immersed single rod case: lower fuel content and higher emulsion content

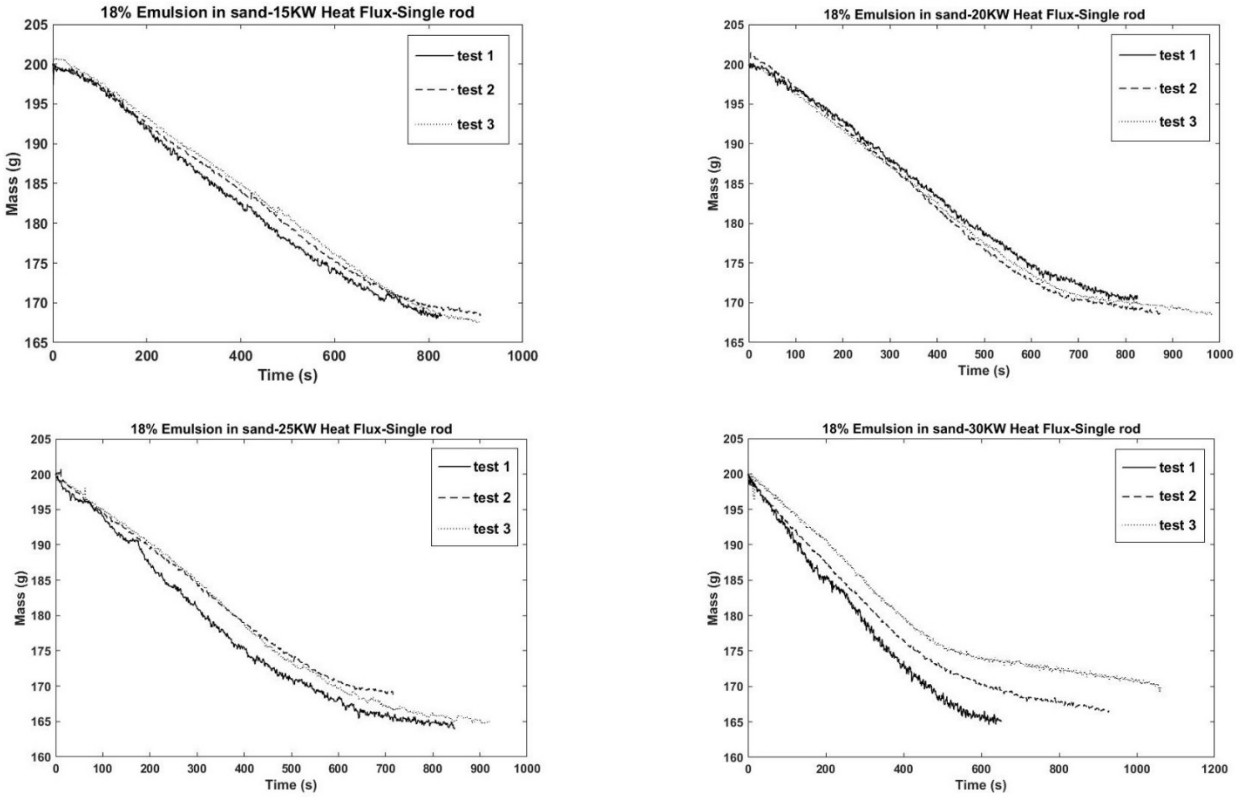

Figure A 3: Mass loss – single immersed rod case (lower emulsion content)

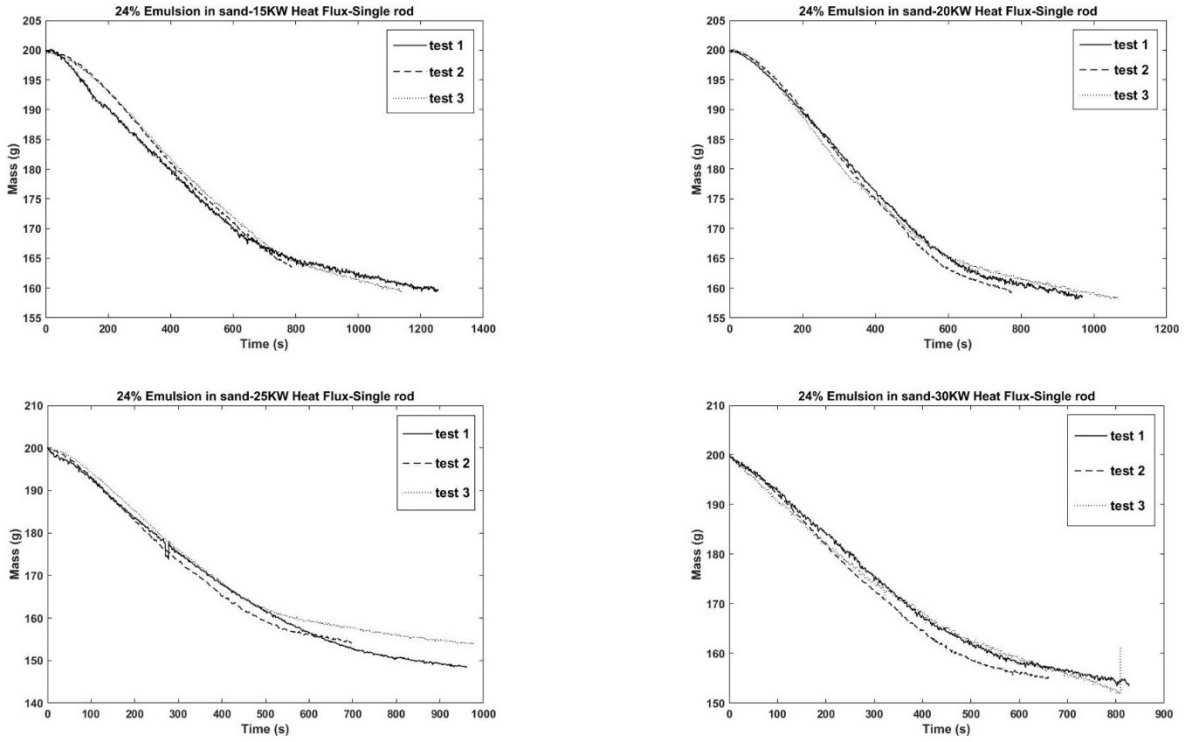

Figure A 4: Mass loss – single immersed rod case (higher emulsion content)

iii. multiple immersed rod cases: lower emulsion content and higher emulsion content

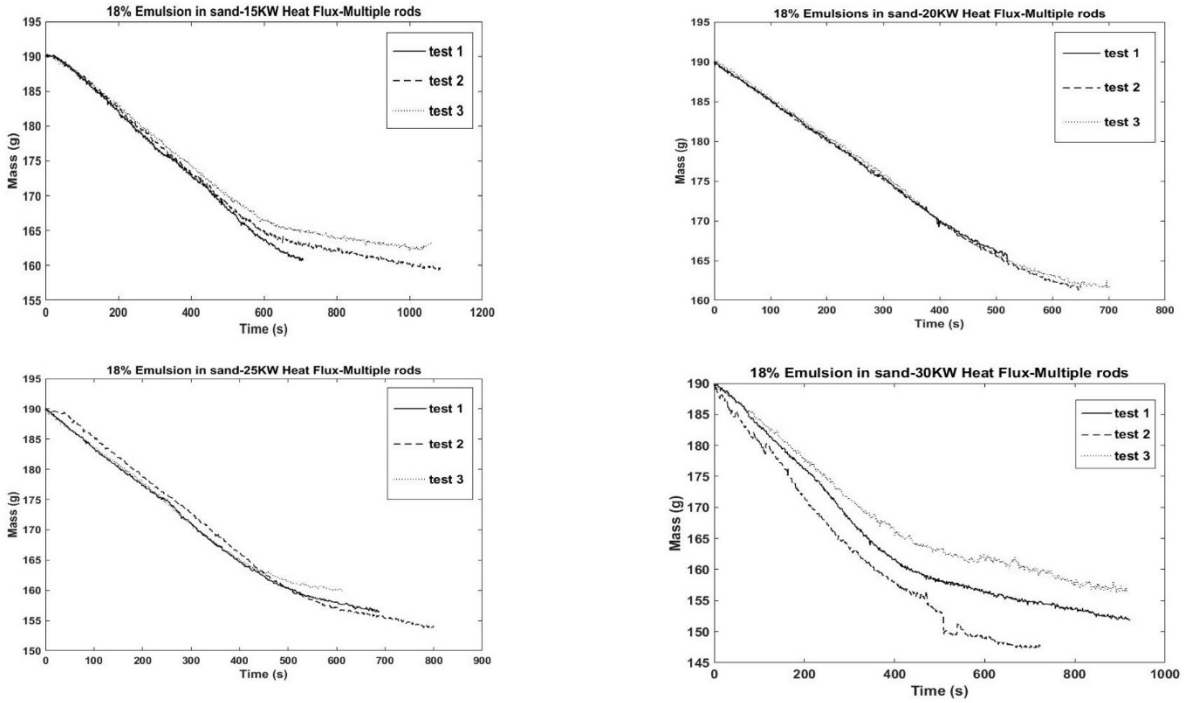

Figure A 5: Mass loss – multiple immersed rods cases (lower emulsion content)

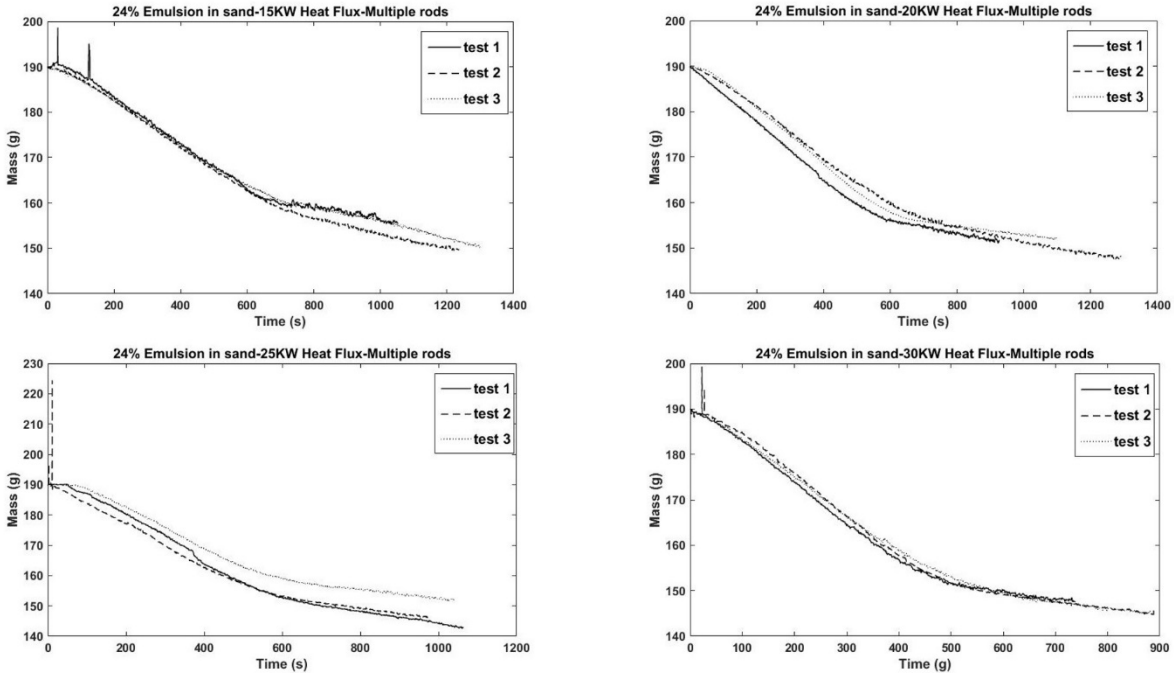

Figure A 6: Mass loss – Multiple immersed rods cases (higher emulsion content)

Temperature profile

1. Low emulsion fuel mixture (18% emulsion and 82% sand) at 30kW/m^2 Heat flux

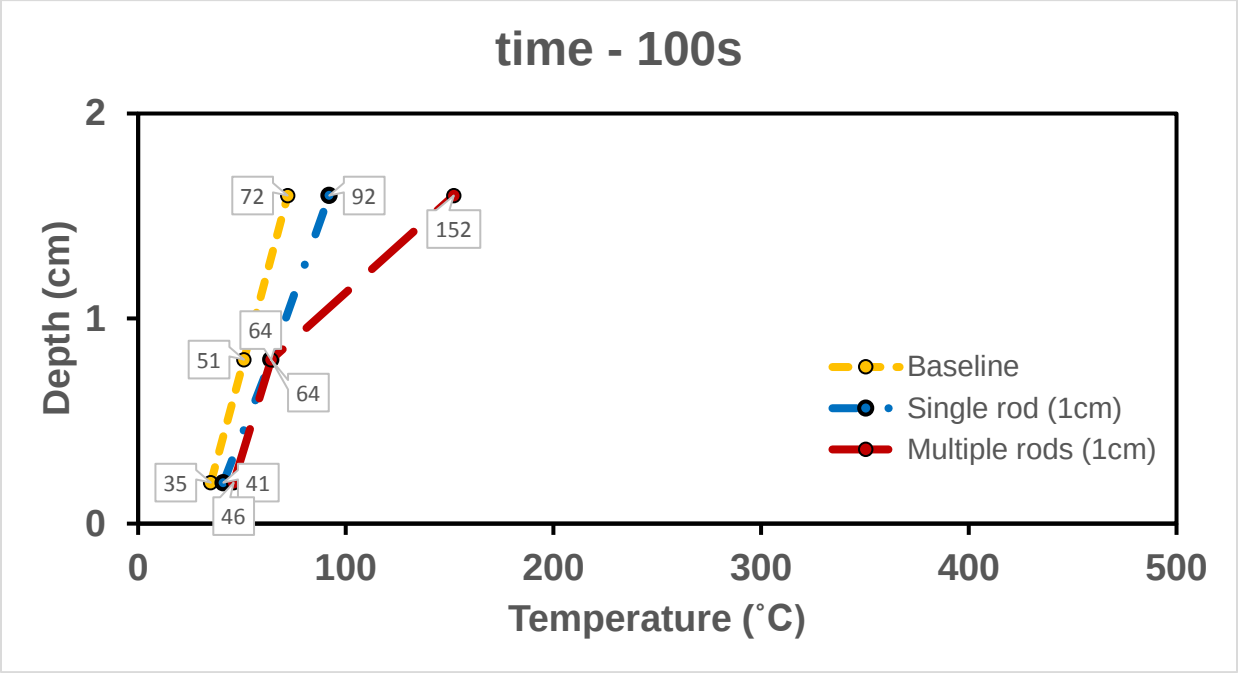

***Figure A 7**: Temperature distribution inside the fuel at 100s*

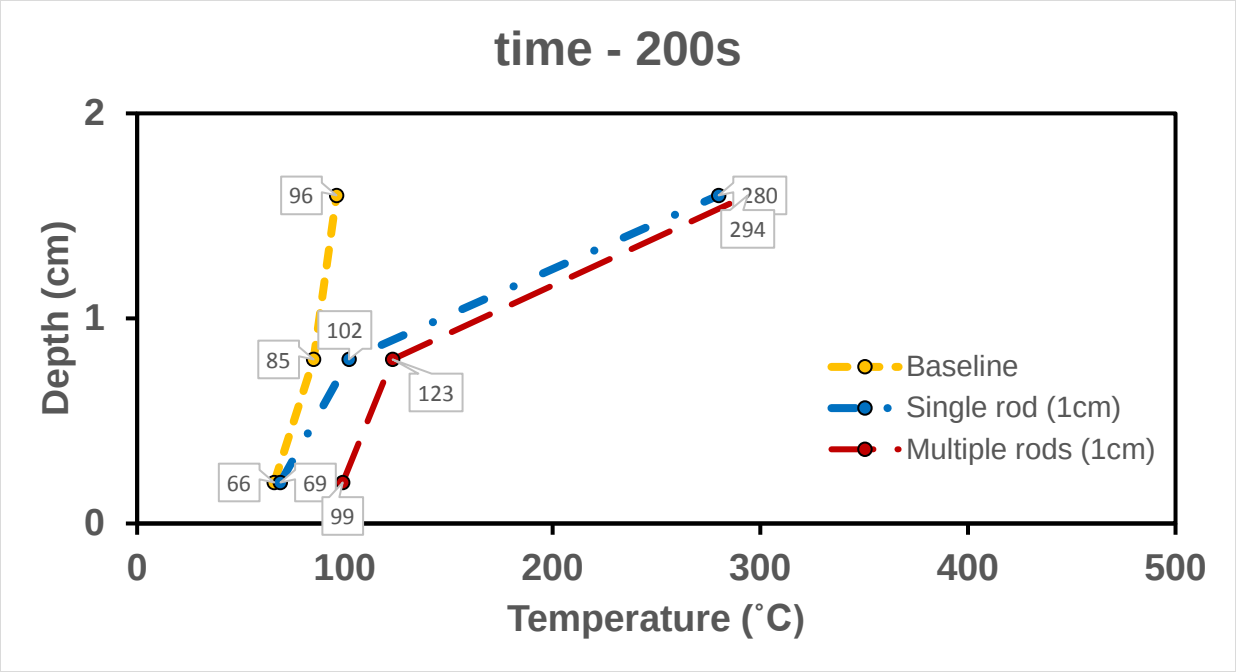

Figure A 8: Temperature distribution inside the fuel at 200s

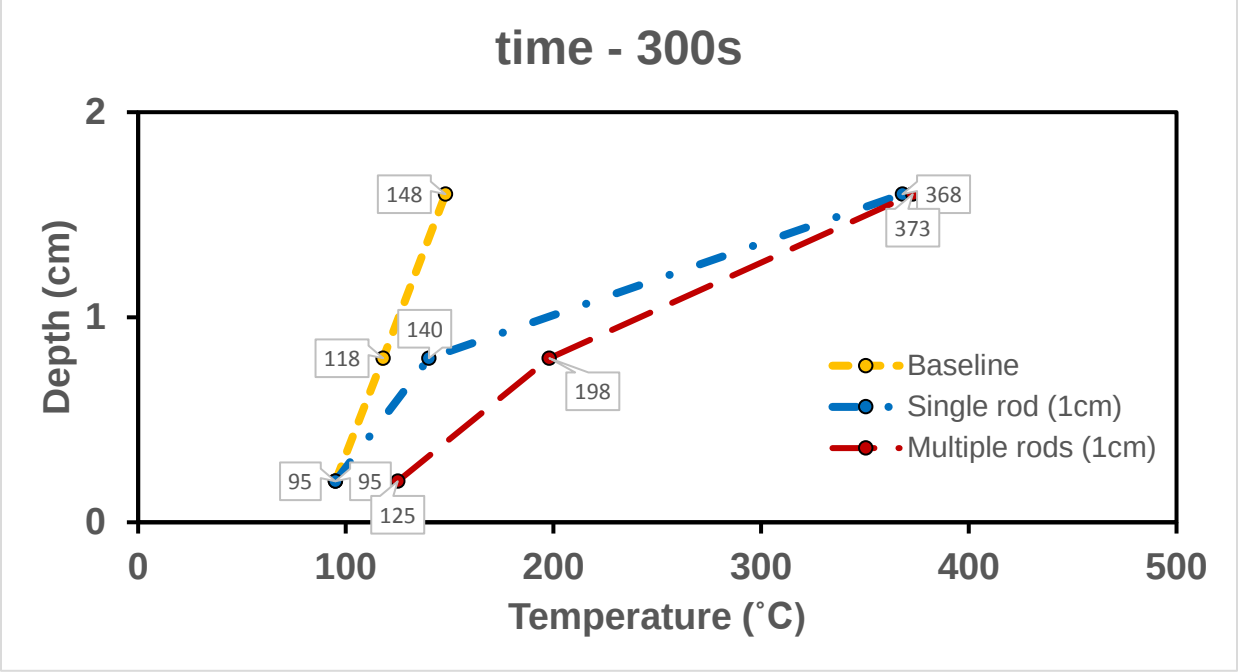

Figure A 9: Temperature distribution inside the fuel at 300s

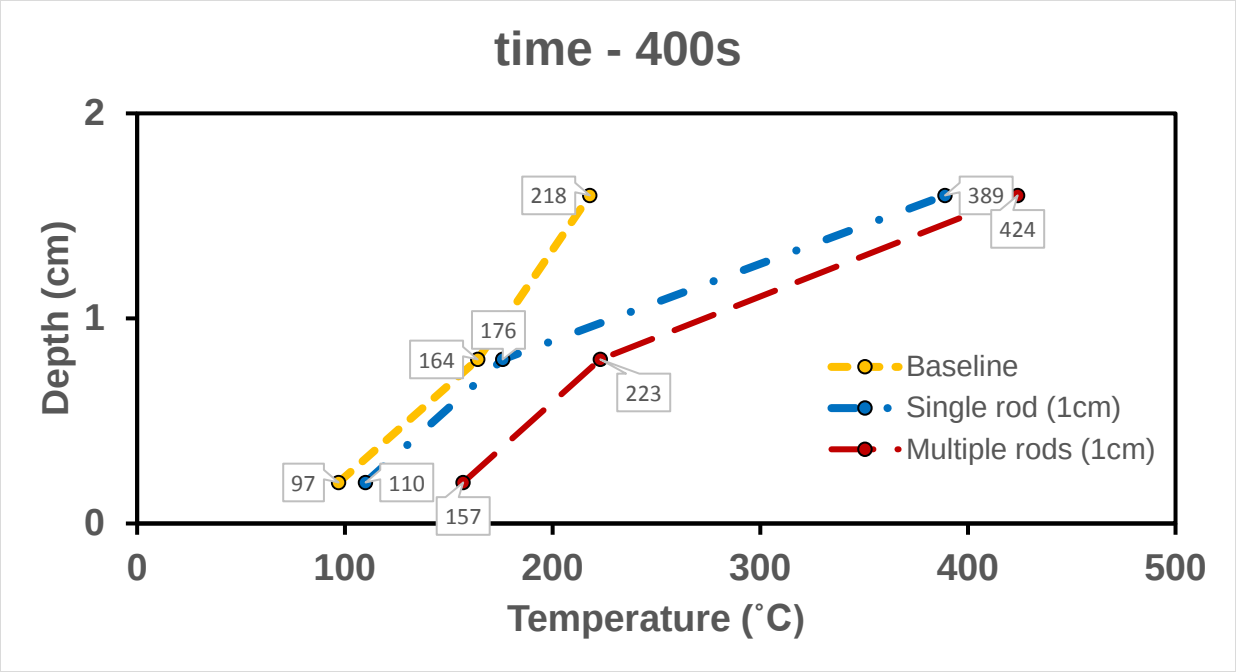

Figure A 10: Temperature distribution inside the fuel at 400s

2. High emulsion fuel mixture (24% emulsion and 76% sand) at 15kW/m^2 Heat flux

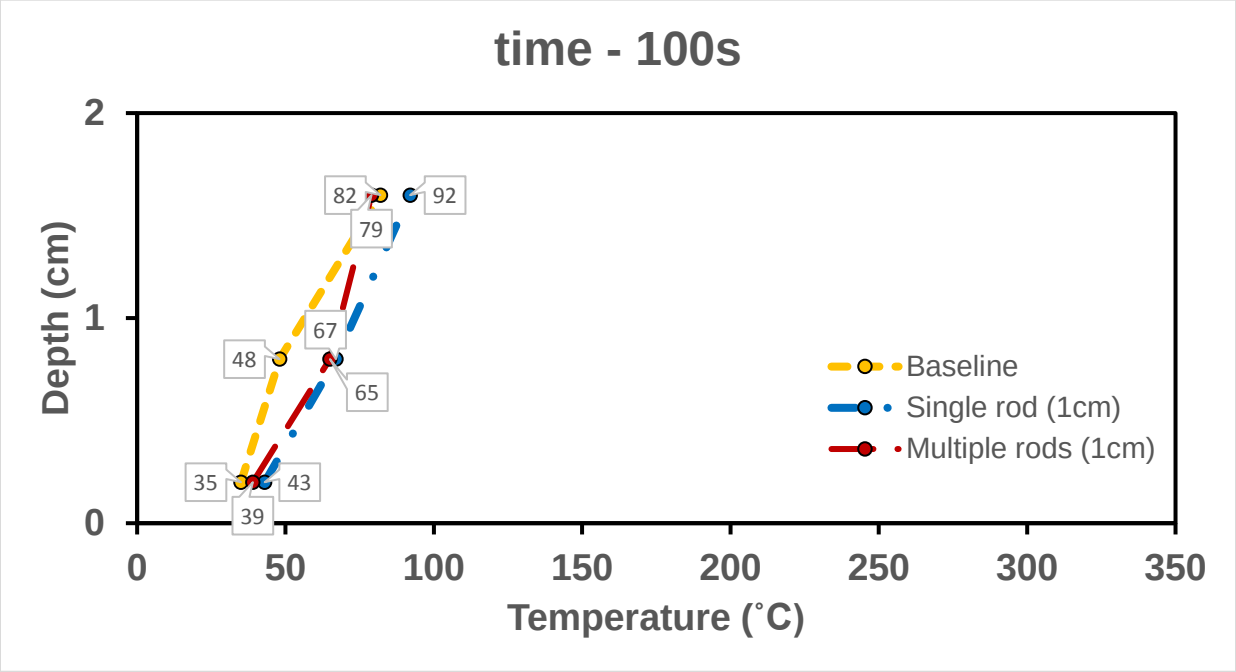

Figure A 11: Temperature distribution inside the fuel at 100s

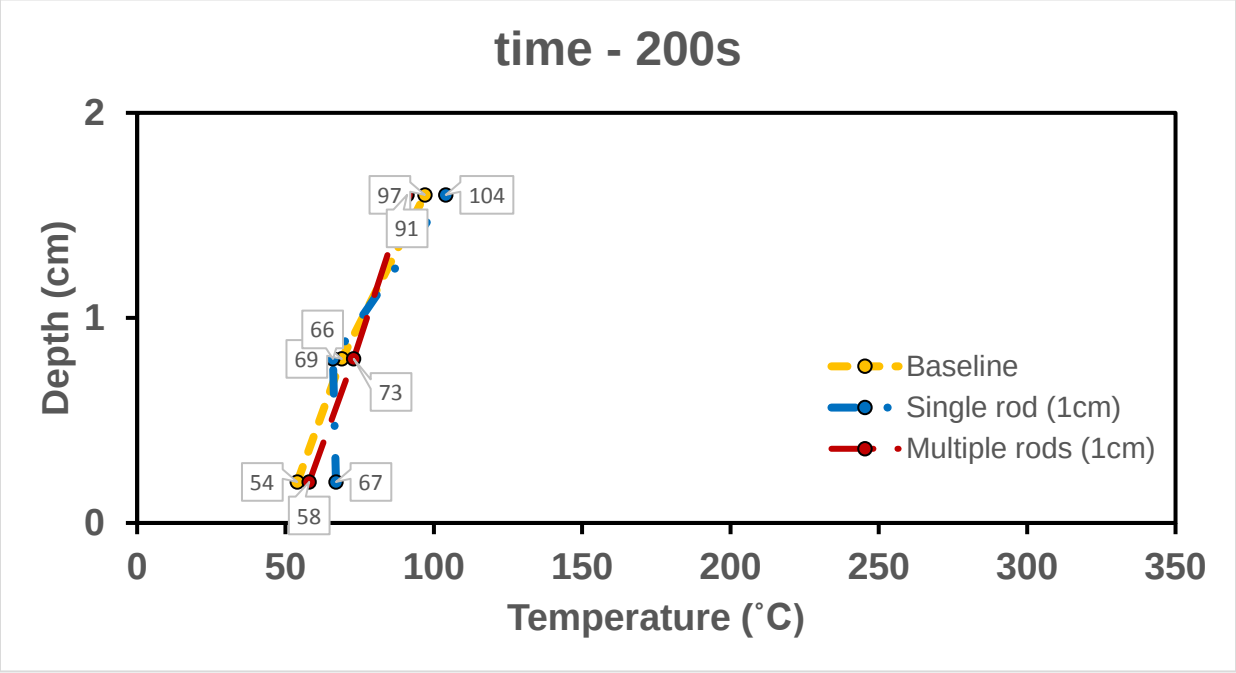

Figure A 12: Temperature distribution inside the fuel at 200s

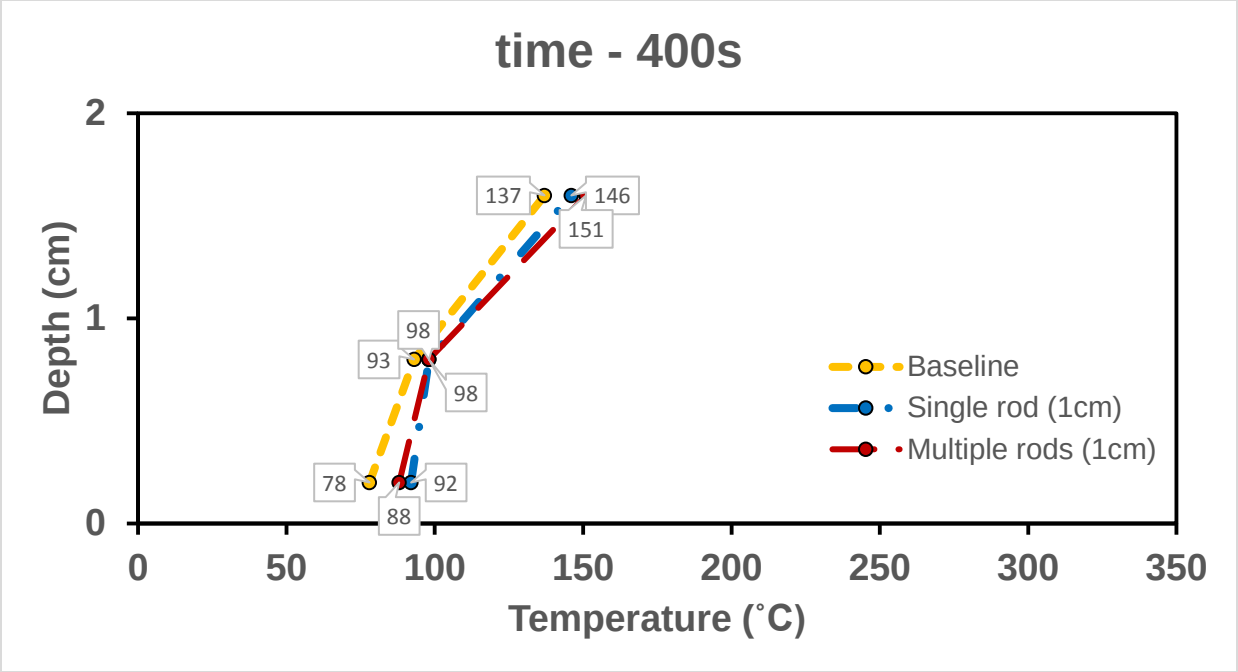

Figure A 13: Temperature distribution inside the fuel at 400s

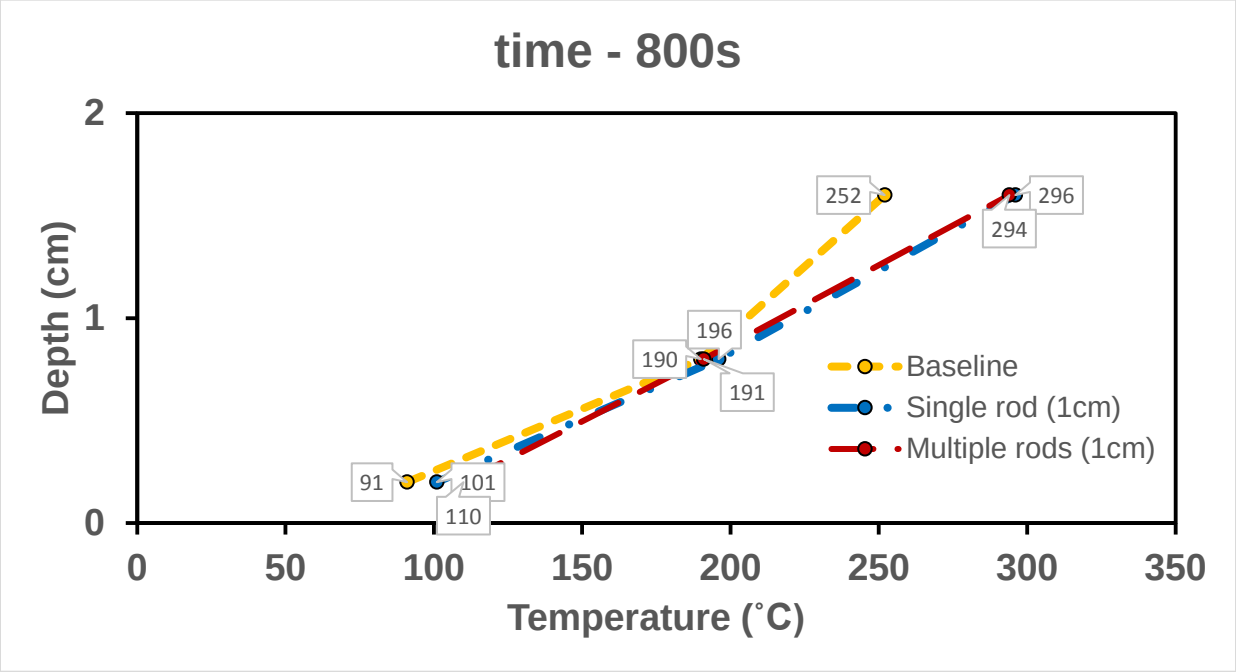

Figure A 14: Temperature distribution inside the fuel at 800s

3. High emulsion fuel mixture (24% emulsion and 76% sand) at 30kW/m^2 Heat flux

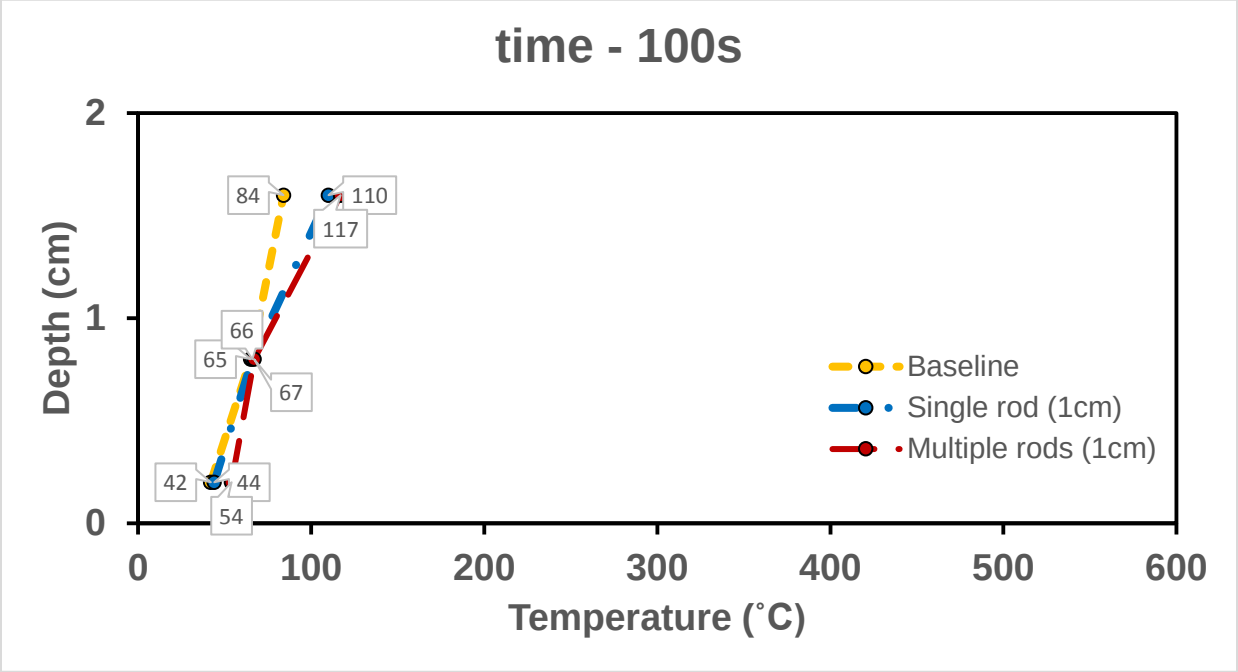

Figure A 15: Temperature distribution inside the fuel at 100s

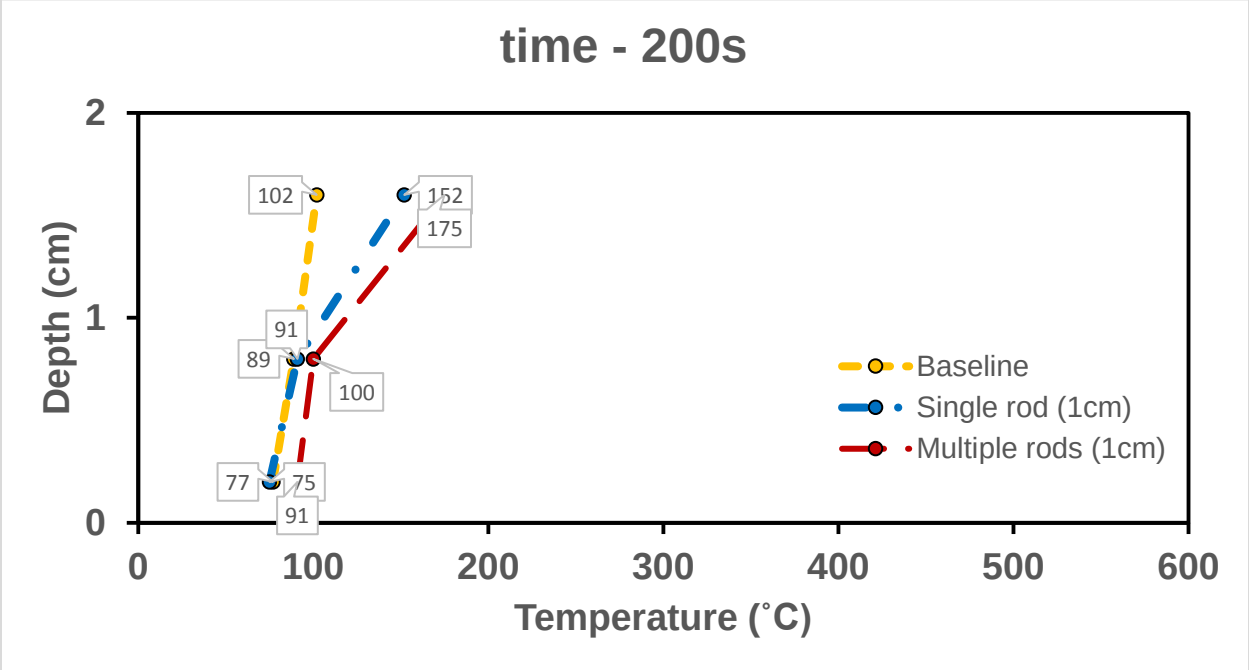

Figure A 16: Temperature distribution inside the fuel at 200s

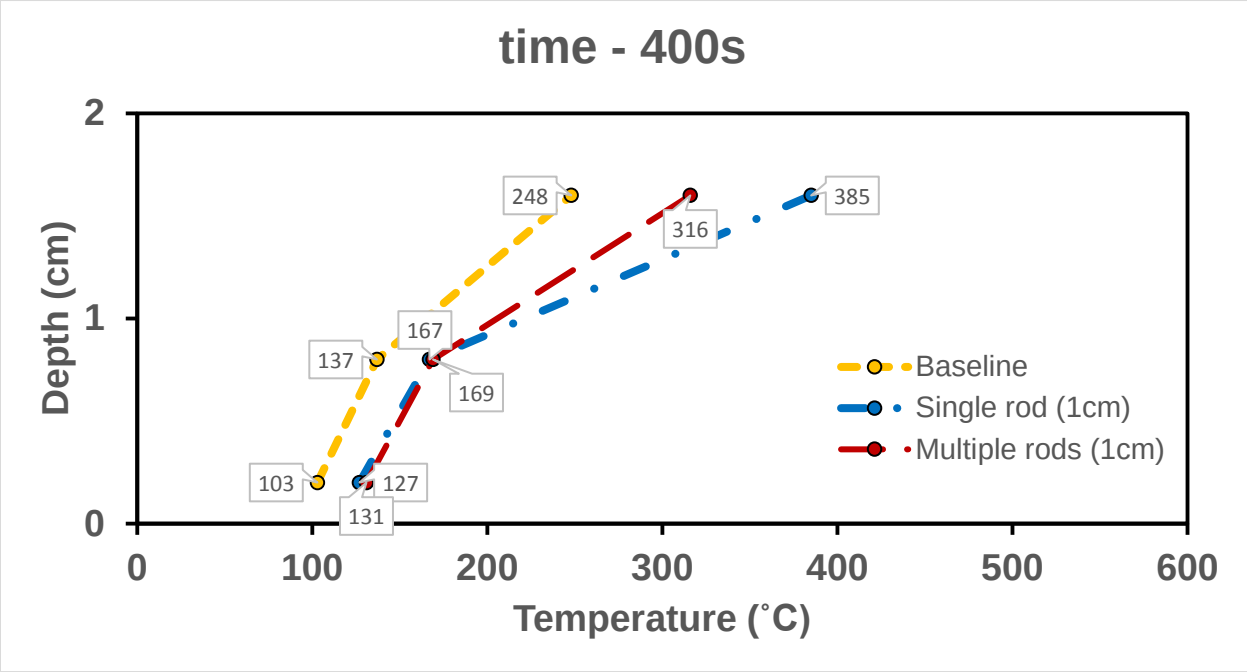

Figure A 17: Temperature distribution inside the fuel at 400s

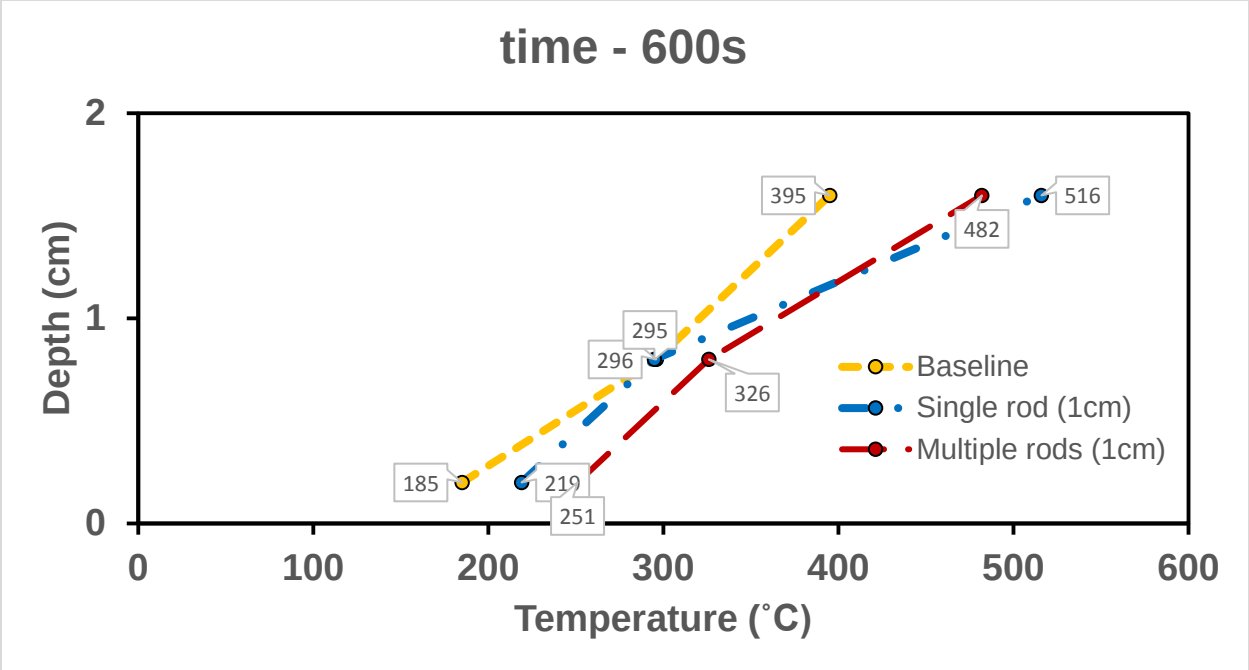

Figure A 18: Temperature distribution inside the fuel at 600s